A hybrid polyketide-nonribosomal peptide in nematodes that promotes larval survival

Qingyao Shou†, Likui Feng†, Yaoling Long, Jungsoo Han, Joshawna K. Nunnery, David H. Powell, Rebecca A. Butcher*

Department of Chemistry, University of Florida, Gainesville, FL 32611

*Correspondence to: butcher@chem.ufl.edu

†equal contributions

Polyketides and nonribosomal peptides are two important classes of natural products that are produced by many species of bacteria and fungi, but are exceedingly rare in metazoans. Here, we elucidate the structure of a hybrid polyketide-nonribosomal peptide from *Caenorhabditis elegans* that is produced in the CAN neurons and promotes survival during starvation-induced larval arrest. Our results uncover a novel mechanism by which animals respond to nutrient fluctuations to extend survival.

Polyketides and nonribosomal peptides represent two of the most important classes of natural products used in modern medicine. They include avermectin, whose derivative ivermectin is used to treat parasitic worms in over 300 million people annually, the antibiotic vancomycin, which is used to treat life-threating infections by gram-positive bacteria, and the immunosuppressant FK506, an essential drug after organ transplantation[1]. These natural products are biosynthesized by polyketide synthases (PKSs) and nonribosomal peptide synthetases (NRPSs), modular megasynthases that function in either an assembly-line or iterative manner[2]. Although PKS and NRPS genes are commonly found in many bacterial and fungal species, only simple, single-module PKSs and NRPSs are present in a few animal species[3,4]. Thus, it is quite remarkable that the genome of the nematode *C. elegans* encodes a huge (865 kDa), multi-module hybrid PKS/NRPS on the X chromosome (PKS-1) and a large (333 kDa), multi-module NRPS on chromosome III (NRPS-1)[5,6]. Homologs of PKS-1 and NRPS-1 are present in most nematode species, including parasitic ones (**Supplementary Results, Supplementary Fig. 1**)[5]. Here, we elucidate the chemical structure of the polyketide-nonribosomal peptide produced by PKS-1/NRPS-1 and show that this natural product promotes recovery from and survival during starvation-induced larval arrest.

We used comparative, untargeted metabolomics to identify the masses of the natural products that PKS-1 and NRPS-1 produce. Extracts from worms and from conditioned culture medium were generated from mixed-stage cultures of wild-type worms, *pks-1* mutant worms, and *nrps-1* mutant worms. The metabolites in the extracts were analyzed by HR-LC-MS and compared using XCMS (**Fig. 1a,b**)[7]. Two peaks (*m/z* 757.3866 and 755.3700), termed nemamide A (**1**) and nemamide B (**2**), respectively, were present in wild-type worm extracts and completely absent in <u>*both*</u> mutant worm extracts (**Supplementary Fig. 2**). Thus, PKS-1 and NRPS-1 likely work

together to make a hybrid polyketide-nonribosomal peptide. Nemamide A and B are associated with the worm body rather than secreted into the culture medium, as the molecules were not detected by HR-LC-MS in the culture medium extracts.

To purify enough of the nemamides to identify their structures by NMR spectroscopy, wild-type worms were grown in an axenic, semi-defined medium[8] that gives a much higher density of worms than bacteria-fed worm cultures. We grew ~50L of worm culture, and ultimately, we estimate that we purified only ~70 μg of nemamide A and less of nemamide B. These compounds were extracted from freeze-dried worms and purified using a short silica gel column, followed by an HP-20 column, a Sephadex LH-20 column, and then HPLC. The extraction and purification process had to be completed for small batches of worms (from ~2L of culture) within 1-2 days to prevent degradation of the nemamides. The exact masses of nemamide A and B indicated the molecular formulas $C_{34}H_{54}N_8O_{10}$ and $C_{34}H_{52}N_8O_{10}$, respectively. NMR spectra, including dqf-COSY, TOCSY, HSQC, HMBC, and ROESY spectra, were obtained for nemamide A and used to determine its molecular connectivity (**Supplementary Table 1, Supplementary Fig. 3 and 4**).

Marfey's method[9] was used to establish that nemamide A contains one L-Asn and two D-Asn (**Online Methods**). The relative configurations of the six stereocenters in nemamide A were determined using coupling constants and ROESY correlations (**Supplementary Figs. 5-7**). The absolute configurations of the four stereocenters in the macrolactam ring were determined by chemically synthesizing three model cyclic peptides with the three possible configurations (2*S*,6*R*,10*R*,18*R*, 2*R*,6*S*,10*R*,18*S*, and 2*R*,6*R*,10*S*,18*S*) and comparing their NMR spectra to that of nemamide A (**Supplementary Fig. 8, Supplementary Tables 2 and 3**). Additional support for the absolute configurations of the stereocenters at C-20 and C-22 was obtained through comparison of the observed CD spectrum of nemamide A to a predicted CD spectrum (**Supplementary Fig.**

9). Additional support was also provided by analysis of the ketoreductase (KR) domain responsible for installing the C-22 stereocenter (see discussion of biosynthesis below). Thus, we propose that the absolute configuration of nemamide A is 2*S*,6*R*,10*R*,18*R*,20*R*,22*S* (**Fig. 1c**). In comparison to nemamide A, nemamide B has one additional double bond, based on its NMR spectra, HR-MS, MS/MS, and UV spectrum (**Fig. 1c, Supplementary Fig. 10-12**).

Although the nemamide structures could not be predicted from the protein sequences of PKS-1 and NRPS-1, they are largely consistent with the domain architectures of the megasynthases. Biosynthesis begins on PKS-1, which initially extends the growing natural product through six iterative cycles, then uses two additional PKS modules to further extend the polyketide in an assembly-line manner, and then uses the C-terminal NRPS module to incorporate β-Ala (**Fig. 1d**). Next, the growing natural product is passed to NRPS-1, which sequentially adds D-Asn, D-Asn, and L-Asn and then forms the macrolactam ring (**Fig. 1d**). The biosynthetic pathway, however, has several non-canonical features, including (1) KR domains (specifically, KR_2 and KR_3) that cannot be classified as A-type or B-type, which would enable their stereospecificities to be predicted (**Fig. 1d, Supplementary Fig. 13**)[10], (2) Missing enzymatic domains, such as methyltransferase and aminotransferase domains, that are likely encoded elsewhere in the *C. elegans* genome (**Fig. 1d**)[11], (3) Adenylation domains with protein sequences that diverge significantly from those of bacterial and fungal adenylation domains (**Fig. 1d, Supplementary Table 4**)[12], (4) The absence of any obvious epimerase domains[2] despite the presence of D-Asn in the nemamides (**Fig. 1d**), and (5) A chain-terminating thioesterase domain present not only at the C-terminus of NRPS-1, but also, unusually, at the C-terminus of PKS-1 (**Fig. 1d, Supplementary Figs. 14** and **15**)[2,13].

Using transcriptional reporter strains, we showed that *pks-1* and *nrps-1* are expressed during all larval stages and the adult stage specifically in the CAN neurons, two essential neurons with a poorly defined role that extend the length of the worm and are closely associated with the excretory canals (**Fig. 2a,b**)[14]. Given that *pks-1* and *nrps-1* are expressed neuronally, we speculated that the nemamides might play a signaling role in development. With sufficient food (bacteria), *C. elegans* will progress from the egg, through four larval stages (L1-L4) to the adult. However, if *C. elegans* eggs hatch to L1 larvae in the complete absence of food, the L1 larvae will arrest, but then resume development upon addition of food[15]. The *pks-1* and *nrps-1* arrested L1s recovered much slower than wild-type arrested L1s when placed on food **(Fig. 2c)**. The mutants progress from the egg to the L4 stage at the same rate as wild-type worms (**Supplementary Fig. 16**), and thus, do not have a general defect in larval progression or development, but rather a specific defect in recovery from L1 arrest. Additionally, the *pks-1* and *nrps-1* mutants enter and recover from the dauer larval stage as well as wild type (**Supplementary Fig. 17**). Like wild-type worms, the *pks-1* and *nrps-1* mutants maintain proper somatic progenitor cell and germline arrest during L1 arrest (**Supplementary Fig. 18 and 19**). Thus, although the *pks-1* and *nrps-1* mutants are defective in recovery from L1 arrest, they are not defective in L1 arrest initiation and maintenance[16].

The insulin/IGF-1 pathway is an important regulator of L1 arrest and recovery, and specific insulins are down-regulated upon L1 arrest and then up-regulated following food addition[15,17,18]. To determine whether the nemamides affect insulin expression, we profiled the expression of all 40 *C. elegans* insulins by qRT-PCR during L1 arrest and recovery. In the *pks-1* and *nrps-1* arrested L1s, *ins-4*, *ins-5*, *ins-19*, and *ins-37* are expressed at higher levels than in wild-type arrested L1s (**Supplementary Fig. 20**). Furthermore, unlike in wild type, in the *pks-1* and *nrps-1* backgrounds,

ins-5 and *ins-19* are not induced during L1 recovery and *ins-4* and *ins-37* are down-regulated during L1 recovery (**Fig. 2d, Supplementary Fig. 21**). The production of the nemamides decreases during L1 recovery (**Supplementary Fig. 22**). Thus, our data suggest that the nemamides are negative regulators of the expression of specific insulins, such that expression of these insulins increases as nemamide levels decrease during L1 recovery.

The *pks-1* and *nrps-1* mutants show reduced survival during prolonged L1 arrest (**Fig. 2e, Supplementary Fig. 23**). Although it has been shown that L1 survival is density-dependent and that L1s secrete unidentified small molecules that increase survival[19], the nemamides are unlikely to be a component of this pheromone, since the mutants showed reduced survival relative to wild type, regardless of worm density (**Supplementary Fig. 24**). *C. elegans* mutants which eat less display reduced survival during L1 arrest[15]. However, the *pks-1* and *nrps-1* mutants are not defective in bacterial food consumption or pharynx pumping (**Supplementary Figs. 25** and **26**), and thus, their reduced survival is not simply due to reduced nutrient stores. Because the insulin/IGF-1 pathway regulates L1 survival, we investigated the genetic interactions between this pathway and the nemamide pathway. Performing the survival assay in insulin/IGF-1 pathway mutant backgrounds suggests that although nemamide signaling regulates insulin expression, it functions at least partially independently of the insulin/IGF-1 pathway (**Fig. 2e, Supplementary Fig. 27**)[15].

The mechanisms by which animals control their development and physiology in response to nutrient fluctuations are poorly understood. The nemamides could potentially serve as a chemical tool with which to dissect this process. We show that the nemamides are important for survival during and recovery from starvation-induced larval arrest. The nemamides likely influence larval development in *C. elegans* in part by modulating insulin signaling

(**Supplementary Fig. 28**). The nemamides represent the first polyketide-nonribosomal peptides biosynthesized in an assembly-line manner in a metazoan. Their discovery will enable the exploration of polyketide and nonribosomal peptide biosynthesis in the context of a complex animal system. Nemamide biosynthesis likely requires additional enzymes that act in *trans*. Future studies of the site of expression and regulation of these enzymes could potentially provide additional insights into the biological role and site of action of the nemamides. As the nemamide biosynthetic genes are found in most nematode species, including parasitic ones, the role of the nemamides in larval development is likely conserved across nematode evolution.

Acknowledgements

We thank Andy Fire, Alison Frand, Nadeem Moghal, and Piali Sengupta for plasmids, Jim Rocca for help with NMR acquisition, Jodie Johnson for MS-MS analysis, Yousong Ding and Yi Zhang for help with Sybyl software, Steve Hagan, Gail Fanucci, and Zhanglong Liu for help with CD spectroscopy, and Yu Zhu for help with calculating CD spectra. We acknowledge the CGC, which is funded by the NIH Office of Research Infrastructure Programs (P40 OD010440), and the NemaGENETAG consortium for providing strains. This work was supported by funds to R.A.B. from the NIH (GM118775), the NSF (1555050), the Ellison Medical Foundation (AG-NS-0963-12), the Alfred P. Sloan Foundation (BR2014-071), and the National High Magnetic Field Laboratory, which is supported by NSF Cooperative Agreement No. DMR-1157490 and the State of Florida.

Author Contributions

Q.S. purified and structurally characterized the nemamides. L.F. generated transgenic worm strains and performed biological assays. Y.L. performed metabolomic analyses. J.H. generated extracts. J.K.N. analyzed nemamide stability. Q.S., L.F., Y.L., D.H.P., and R.A.B. analyzed the data. R.A.B., Q.S., and L.F. wrote the manuscript.

Competing Financial Interests

The authors declare no competing financial interests.

References

1 Omura, S. & Crump, A. Ivermectin: panacea for resource-poor communities? *Trends Parasitol.* **30**, 445-455 (2014).

2 Fischbach, M. A. & Walsh, C. T. Assembly-line enzymology for polyketide and nonribosomal Peptide antibiotics: logic, machinery, and mechanisms. *Chem. Rev.* **106**, 3468-3496 (2006).

3 Castoe, T. A., Stephens, T., Noonan, B. P. & Calestani, C. A novel group of type I polyketide synthases (PKS) in animals and the complex phylogenomics of PKSs. *Gene* **392**, 47-58 (2007).

4 Hojo, M. *et al.* Unexpected link between polyketide synthase and calcium biomineralization. *Zoological Letters* **1**, 1-16 (2015).

5 O'Brien, R. V., Davis, R. W., Khosla, C. & Hillenmeyer, M. E. Computational identification and analysis of orphan assembly-line polyketide synthases. *J. Antibiot. (Tokyo)* **67**, 89-97 (2014).

6 Wang, H., Fewer, D. P., Holm, L., Rouhiainen, L. & Sivonen, K. Atlas of nonribosomal peptide and polyketide biosynthetic pathways reveals common occurrence of nonmodular enzymes. *Proc. Natl. Acad. Sci. U. S. A.* **111**, 9259-9264 (2014).

7 Gowda, H. *et al.* Interactive XCMS Online: simplifying advanced metabolomic data processing and subsequent statistical analyses. *Anal. Chem.* **86**, 6931-6939 (2014).

8 Nass, R. & Hamza, I. The nematode *C. elegans* as an animal model to explore toxicology in vivo: solid and axenic growth culture conditions and compound exposure parameters. *Curr. Protoc. Toxicol.* **Chapter 1**, Unit1 9 (2007).

9 Bhushan, R. & Brückner, H. Marfey's reagent for chiral amino acid analysis: a review. *Amino Acids* **27**, 231-247 (2004).

10 Kwan, D. H. & Schulz, F. The stereochemistry of complex polyketide biosynthesis by modular polyketide synthases. *Molecules* **16**, 6092-6115 (2011).

11 Aron, Z. D., Dorrestein, P. C., Blackhall, J. R., Kelleher, N. L. & Walsh, C. T. Characterization of a new tailoring domain in polyketide biogenesis: the amine

transferase domain of MycA in the mycosubtilin gene cluster. *J. Am. Chem. Soc.* **127**, 14986-14987 (2005).
12 Rottig, M. *et al.* NRPSpredictor2--a web server for predicting NRPS adenylation domain specificity. *Nucleic Acids Res.* **39**, W362-367 (2011).
13 Du, L. & Lou, L. PKS and NRPS release mechanisms. *Nat. Prod. Rep.* **27**, 255-278 (2010).
14 Forrester, W. C., Perens, E., Zallen, J. A. & Garriga, G. Identification of *Caenorhabditis elegans* genes required for neuronal differentiation and migration. *Genetics* **148**, 151-165 (1998).
15 Baugh, L. R. To grow or not to grow: nutritional control of development during *Caenorhabditis elegans* L1 arrest. *Genetics* **194**, 539-555 (2013).
16 Fukuyama, M., Kontani, K., Katada, T. & Rougvie, A. E. The *C. elegans* Hypodermis Couples Progenitor Cell Quiescence to the Dietary State. *Curr. Biol.* **25**, 1241-1248 (2015).
17 Lee, B. H. & Ashrafi, K. A TRPV channel modulates *C. elegans* neurosecretion, larval starvation survival, and adult lifespan. *PLoS Genet.* **4**, e1000213 (2008).
18 Chen, Y. & Baugh, L. R. *Ins-4* and *daf-28* function redundantly to regulate *C. elegans* L1 arrest. *Dev Biol* **394**, 314-326 (2014).
19 Artyukhin, A. B., Schroeder, F. C. & Avery, L. Density dependence in *Caenorhabditis* larval starvation. *Sci. Rep.* **3**, 2777 (2013).
20 Frand, A. R., Russel, S. & Ruvkun, G. Functional genomic analysis of *C. elegans* molting. *PLoS Biol.* **3**, e312 (2005).
21 Baugh, L. R. & Sternberg, P. W. DAF-16/FOXO regulates transcription of *cki-1*/Cip/Kip and repression of *lin-4* during *C. elegans* L1 arrest. *Curr. Biol.* **16**, 780-785 (2006).

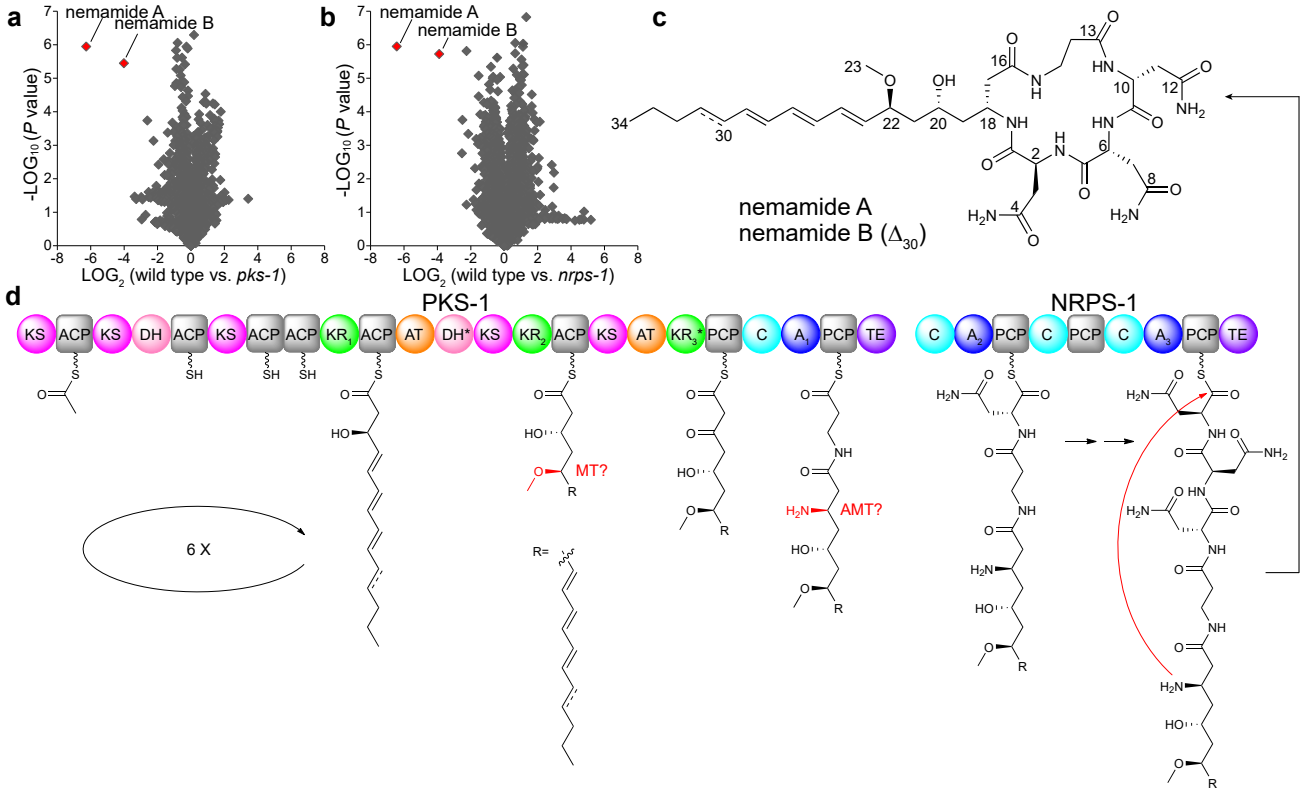
a
nemamide A
nemamide B
-LOG10 (P value)
LOG2 (wild type vs. pks-1)
b
nemamide A
nemamide B
-LOG10 (P value)
LOG2 (wild type vs. nrps-1)
c
nemamide A
nemamide B (Δ30)
d
PKS-1
NRPS-1
KS ACP KS DH ACP KS ACP ACP KR1 ACP AT DH* KS KR2 ACP KS AT KR3* PCP C A1 PCP TE
C A2 PCP C PCP C A3 PCP TE
6 X
MT?
AMT?
R=

Figure 1. Discovery and biosynthesis of the nemamides. (**a**,**b**) Comparison of average peak areas for metabolite features in wild-type worms versus *pks-1* mutant worms (**a**) and in wild-type worms versus *nrps-1* mutant worms (**b**), with nemamide A and B highlighted in red. In **a** and **b**, extracts from three separate cultures were analyzed for each strain, and *P* values were calculated in XCMS using a Welch's t-test. (**c**) Chemical structures of nemamide A and B. (**d**) Proposed biosynthetic assembly line for the nemamides. Domain abbreviations: acyl transferase (AT), acyl carrier protein (ACP), ketosynthase (KS), ketoreductase (KR), dehydratase (DH), methyltransferase (MT), aminotransferase (AMT), adenylation (A), peptidyl carrier protein (PCP), condensation (C), and thioesterase (TE). Domains labeled with an asterisk are predicted to be inactive based on the nemamide structures. The KR and A domains are labeled with numbers for further discussion in **Supplementary Figure 13 and Supplementary Table 4**. KR_1 is predicted to be B-type, while KR_2 and KR_3 are neither A- nor B-type (**Supplementary Fig. 13**). Given that the nemamides contain four amino acids and that PKS-1 and NRPS-1 have only three A domains, A_2 may act twice to incorporate two Asn residues.

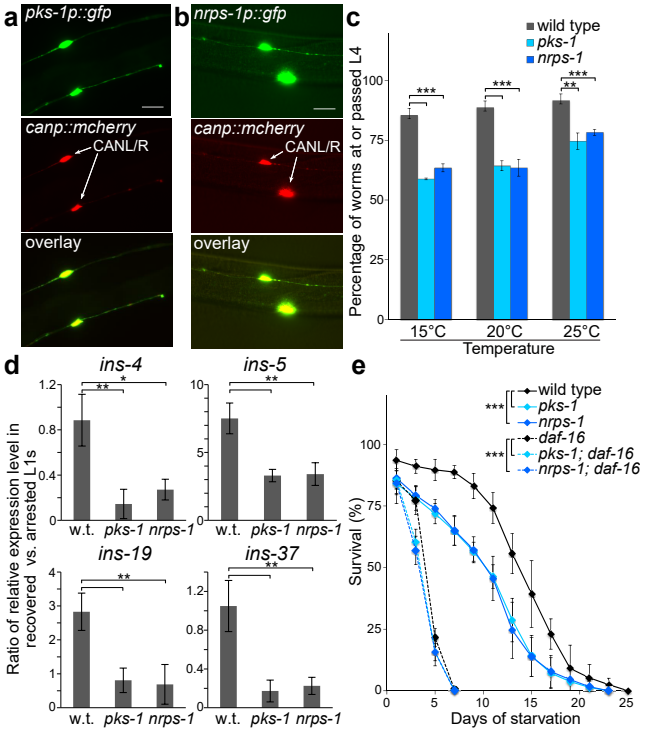
a
pks-1p::gfp
canp::mcherry
CANL/R
overlay
b
nrps-1p::gfp
canp::mcherry
CANL/R
overlay
c
wild type
pks-1
nrps-1
Percentage of worms at or passed L4
15°C
20°C
25°C
Temperature
d
ins-4
ins-5
ins-19
ins-37
Ratio of relative expression level in recovered vs. arrested L1s
w.t. pks-1 nrps-1
e
wild type
pks-1
nrps-1
daf-16
pks-1; daf-16
nrps-1; daf-16
Survival (%)
Days of starvation

Figure 2. Site of expression and biological role of the nemamides. (**a,b**) Expression of the transcriptional reporters *pks-1p::gfp* (**a**) or *nrps-1p::gfp* (**b**), as well as *canp::mcherry* (marker for CAN neurons), in transgenic worms. Scale bar, 20 μm. We obtained similar results for *pks-1p::gfp-pest* and *nrps-1p::gfp-pest* reporters, in which GFP undergoes rapid turnover[20]. (**c**) Recovery of arrested L1s and development to the L4 stage for wild-type, *pks-1*, and *nrps-1* worms at different temperatures. (**d**) Expression of specific insulins in recovered versus arrested wild-type, *pks-1*, and *nrps-1* L1s, as determined by qRT-PCR. (**e**) Survival of wild-type, *pks-1*, and *nrps-1* arrested L1s over time. The insulin/IGF-1 pathway controls L1 survival in a manner dependent on the downstream *daf-16*/*foxo* transcription factor[15,21]. The poor survival of *daf-16*/*foxo (mu86 null)* was slightly enhanced by the *pks-1* and *nrps-1* mutations. Mean survival (days ± SE): 14.3±0.2 for wild type, 11.3±0.3 for *pks-1*, 11.0±0.3 for *nrps-1*, 4.4±0.1 for *daf-16*, 3.7±0.1 for *pks-1; daf-16*, and 3.5±0.1 for *nrps-1; daf-16*. In **c**-**e**, the data represent the mean ± SD of three independent experiments, and two-tailed, unpaired t-tests were applied (*$P \leq 0.05$, **$P \leq 0.01$, ***$P \leq 0.001$).

Online Methods

Strains and culture methods. Worms were maintained on *E. coli* OP50 according to standard methods. Strains used in this study include wild type (N2), *pks-1(ttTi24066)*, *pks-1(ok3769)* (this allele was only used in **Supplementary Fig. 23**), *nrps-1(ttTi45552)*, *pks-1(ttTi24066)*; *nrps-1(ttTi45552)*, *ayIs7*[*hlh-8p::gfp*], *pks-1(ttTi24066); ayIs7*, *nrps-1(ttTi45552); ayIs7*, *unc-31(e928)*, *unc-31(e928); pks-1(ttTi24066)*, *unc-31(e928); nrps-1(ttTi45552), daf-16(mu86)*, *daf-16(mu86); pks-1(ttTi24066)*, and *daf-16(mu86); nrps-1(ttTi45552)*. The *pks-1(ttTi24066)*, *nrps-1(ttTi45552)*, and *pks-1(ok3769)* strains were backcrossed two, four, and four times, respectively. The double mutants were constructed from single mutants using standard genetic methods and the presence of alleles was verified by PCR (**Supplementary Table 5**).

Generation of worm extracts for metabolomic analysis. The wild-type, *pks-1,* and *nrps-1* strains were each grown at room temperature on two NGM agar plates (10 cm) spread with 0.75 mL 25X OP50 until the food on the plates was almost gone. Then, the worms were transferred to 1 L Erlenmeyer flasks containing S medium (350 mL). The worm cultures were grown at 22.5˚C for 3 d and were fed with 3.5 mL of 25X OP50 every day. For sample collection, the culture flasks were placed in an ice-bath for 30 min to 1 h to settle the worms. Then, the worms were transferred from the bottom of the flasks to a 50 mL centrifuge tube and were centrifuged (1000 rpm for 5 min) to separate the worms from the worm medium. After the centrifugation, the supernatant was combined with the worm medium. The process was repeated until most of the worms were removed from the flasks. The collected worms were washed with water three times and centrifuged (1000 rpm for 5 min), and then they were soaked in 10 mL of water for 1 h in a shaking incubator (22.5˚C, 225 rpm) to remove bacteria from their digestive tract. The worms were

collected by centrifugation and were freeze-dried. The dried worm pellets were ground with sea sand (2 g sand per 800–900 mg dried worms) using a mortar and pestle. The ground worms were extracted with 50 mL of ethanol for 1 h, and the extract was filtered through filter paper. The fitrate was collected and dried using a rotovap. The collected worm medium was filtered using Celite and then using a 0.2 μm filter. The medium was extracted with ethyl acetate, and the ethyl acetate layer was then dried using a rotovap. The dried worm and worm media samples were each resuspended in 125 μL of 50% (vol/vol) ethanol in water, sonicated (if needed), and centrifuged (15000 rpm for 1 min) before analysis by HR-LC-MS. In later experiments to attempt to detect the nemamides in culture medium, the culture medium was instead freeze-dried and extracted with 190 proof ethanol.

General methods for chemical analysis. HR-LC-MS analysis was performed on an Agilent 1200 high performance liquid chromatography (HPLC) system equipped with a UV-Vis diode array detector and a 6220 TOF MS using positive ESI in both profile and centroid modes. NMR spectra were recorded on a Varian INOVA 600 equipped with a 1.5 mm microcryoprobe[22], except for an additional HMBC spectrum of nemamide A, which was recorded on a Bruker Avance 800 spectrometer equipped with a 1.7 mm microcryoprobe (**Supplementary Fig. 3i**). CD spectra were obtained on an AVIV-202 CD spectrometer.

Metabolomic analysis. The worm and conditioned medium samples for each worm strain (N2, *pks-1*, and *nrps-1*) each consisted of three biological replicates and two technical replicates. 5 μL of each sample was injected. LC separation was achieved on two Onyx Monolithic C_{18} (Phenomenex, 100 × 4.6 mm, 5 μm) columns in series using a solvent gradient of 1% acetic acid

in water (solvent A) and 1% acetic acid in acetonitrile (solvent B) at a flow rate of 0.33 mL / min. The solvent flow was maintained at 5% B for 6.5 min, then ramped to 100% B over 19 min, then maintained at 100% B for 9.5 min, then ramped to 5% B over 10 min, and maintained at 5% B for 5 min. The mass spectrometer settings include a drying gas flow of 10 L / min, a gas temperature of 325 °C, a nebulizer pressure of 50 psi, a capillary voltage of 4000 V, a fragmentor voltage of 180 V, and a skimmer voltage of 60 V. Worm samples were run in a random order to minimize the impact of mass or retention time shift on the analyses. Data files were converted to mzXML format in centroid mode using ProteoWizard software[23]. Metabolomic comparisons were performed using XCMS Online[7] using the default parameters for HPLC-Q-TOF, except that the "Matched Filter" feature detection method and the "Peak Groups" retention time correction method (with nonlinear alignment) were used.

Purification and characterization of nemamides. Wild-type worms were shaken at 225 rpm for 7 d at 22.5 °C in 2.8 L baffled flasks containing 500 mL of CeHR medium[8] with 20% cow's milk. Worms were collected by centrifugation, washed with water, shaken in water for 30 min to clear their intestines, and washed again with water. Worms were stored frozen at -20 °C until needed. For extraction and fractionation process, worms from 2 L-worth of culture were processed at a time. After freeze drying, worms were ground for 15 min with 70 g of sand using a mortar and pestle. The pulverized worms were transferred to a 1 L Erlenmeyer flask, and 700 mL of 190 proof ethanol was added to the flask. The flask was shaken at 300 rpm for 3.5 h. The extract was filtered using a Buchner funnel and filter paper and evaporated with a rotovap at 27 °C. The extract was then subjected to silica gel chromatography and eluted with a gradient of ethyl acetate/methanol (1:0, 9:1, 1:1, 0:1) to give four fractions (A – D). Fraction D was evaporated

with a rotovap at 27 °C, redissolved in 12 mL of methanol, and centrifuged at 3500 rpm for 10 min. The supernatant was dried and dissolved in 10 mL 70% methanol/water. Fraction D was then applied to an HP-20 column, eluting with MeOH/H2O (7:3 to 9:1) to give four subfractions (D1 – D4). Subfraction D3 was applied to a Sephadex LH-20 column, eluting with methanol to give seven subfractions (D3a – D3g). Fraction D3g, which contained both nemamide A and B based on LC-MS analysis, was further fractionated by HPLC (eclipse XDB-C_{18} column, 150 × 4.6 mm, 5 μm), using a gradient of methanol and water (ramping from 10% to 100% methanol over 30 min, holding at 100% methanol for 6 min, then returning to 10% methanol over 4 min; flow rate 1 mL / min; UV detection at 280 nm), to obtain purified nemamide A and B. Nemamide A: For NMR spectra and ^{1}H and ^{13}C NMR data of nemamide A, see **Supplementary Figure 3** and **Supplementary Table 1**; UV (methanol): λ_{max} 258, 269, 279 nm; HR-ESIMS (*m/z*): $[M+Na]^+$ calcd. for $C_{34}H_{54}N_8O_{10}Na$ 757.3861, found 757.3866. Nemamide B: For NMR spectra, see **Supplementary Figure 12**; UV (methanol): λ_{max} 286, 301, 315 nm; HR-ESIMS (*m/z*): $[M+Na]^+$ calcd. for $C_{34}H_{52}N_8O_{10}Na$ 755.3704, found 755.3700.

Marfey's analysis. Nemamide A (purified from worms from 2.5 L of culture) was hydrolyzed with 200 μL of 6 N HCl at 110 °C for 12 h. The reaction was then dried down by rotovap, and the residue was dissolved in 50 μL of water. 50 mM stock solutions of the amino acid standards (L-Asp, D-Asp, L-Asn, D-Asn) were made in water. 20 μL of 1 M $NaHCO_3$ and 100 μL of 1-fluoro-2,4-dinitrophenyl-5-L-alaninamide (L-FDAA, Marfey's reagent; 1% w/v in acetone) were added to 50 μL of the sample or the amino acid standards. After heating at 37 °C for 60 min, reactions were quenched by addition of 20 μL of 1 N HCl. The sample reaction was diluted with 100 μL of acetonitrile while the reactions of the amino acid standards were diluted with 810 μL of

acetonitrile. The reactions of the sample and standards were subjected to LC-MS analysis (Phenomenex Luna $C_{18,}$ 4.6 × 100 mm, 5 μm) using a linear gradient of water with 0.1% formic acid and acetonitrile with 0.1% formic acid (holding at 10% acetonitrile for 5 min, then ramping to 50% acetonitrile over 30 min; flow rate, 0.7 mL/min; UV and ESI-MS detection, 340 nm and negative ion mode). Analysis with both Asn and Asp amino acids indicated the conversion of Asn to Asp during the acid hydrolysis step for both the sample and the Asn amino acid standards. Retention times for L-FDAA-L-Asp and L-FDAA-D-Asp were 22.0 and 22.7 min, respectively. The extracted ion chromatogram (*m/z* 384) for the sample indicated the presence of L-FDAA-L-Asp and L-FDAA-D-Asp in a 1:2.16 ratio.

Cyclic peptide synthesis. H-β-Ala-2-ClTrl resin was purchased from Novabiochem, and Fmoc-L-Asn(Trt)-OH, Fmoc-D-Asn(Trt)-OH, (*R*)-3-(Fmoc-amino)butyric acid, and (*S*)-3-(Fmoc-amino)butyric acid were purchased from Chem-Impex International. Compound **3** was made through the sequential coupling to the resin of (*R*)-3-(Fmoc-amino)butyric acid, Fmoc-L-Asn(Trt)-OH, Fmoc-D-Asn(Trt)-OH, and Fmoc-D-Asn(Trt)-OH, followed by cleavage from the resin and cyclization. Compound **4** was made through the sequential coupling to the resin of (*S*)-3-(Fmoc-amino)butyric acid, Fmoc-D-Asn(Trt)-OH, Fmoc-L-Asn(Trt)-OH, and Fmoc-D-Asn(Trt)-OH, followed by cleavage from the resin and cyclization. Compound **5** was made through the sequential coupling to the resin of (*S*)-3-(Fmoc-amino)butyric acid, Fmoc-D-Asn(Trt)-OH, Fmoc-D-Asn(Trt)-OH, and Fmoc-L-Asn(Trt)-OH, followed by cleavage from the resin and cyclization. Solid-phase peptide synthesis was conducted in 10 mL BD Luer-Lok syringes. For deprotection, H-β-Ala-2-ClTrl resin (0.25 g, 0.375 mmol/g) was swelled in dry CH_2Cl_2 for 20 min. The resin was treated with 20% (v/v) piperidine / DMF (5 mL) for 30 min and then washed with DMF (3 ×

5 mL). For amino acid coupling, a solution of protected amino acid (5 eq.) in DMF, HOBt (5.5 eq.) in DMF and DIC (5.5 eq.) together with 5 mL CH_2Cl_2 was added to the resin. After 4 h, the resin was washed with DMF (5 mL), CH_2Cl_2 (5 mL), and DMF (5 mL). The reaction was monitored using the ninhydrin test. When the ninhydrin test was negative, deprotection and coupling to the next amino acid was carried out. For cleavage of the linear peptide, the resin was treated with a 5 mL solution of 1,1,1,3,3,3-hexafluoro-2-propanol in CH_2Cl_2 (1:4, v/v) for 30 min. This process was repeated two additional times, and the combined cleavage solution was concentrated in vacuum. For cyclization of the linear peptide, the crude linear peptide (100 mg, 0.08 mmol) was dissolved in 80 mL DMF, and 4-(4,6-dimethoxy-1,3,5-triazin-2-yl)-4-methylmorpholinium tetrafluoroborate ($DMTMM^+$ BF_4^-, 54 mg, 0.16 mmol) and iPr_2NEt (28 µL, 158.6 µmol) was added to the solution. The solution was stirred overnight and then concentrated under reduced pressure using a rotovap. For deprotection of the trityl groups, 10 mL of a solution of TFA, triisopropylsiline, and water (95:2.5:2.5, v/v/v) was added for 2 h, and then concentrated to give the crude cyclic peptide. For purification of the cyclic peptide, the crude cyclic peptide was initially purified on a C_{18} column (50g Octadecyl-functionalized silica gel, 3.5 cm × 50 cm), eluted with 10% methanol, and then further purified using reversed-phase HPLC (0–5 min: 2% acetonitrile, 5–15 min: 2%–30% acetonitrile, 15–20 min: 30% acetonitrile) to afford pure cyclic peptide.

Construction of reporter strains. The PEST sequence from pAF207[20] (gift of Alison Frand) was subcloned into pPD114.108 at the XhoI/EcoRI sites to generate pPD114.108-*gfp::pest*. 4.563 kb of the *pks-1* promoter and 3 kb of the *nrps-1* promoter were amplified from *C. elegans* genomic DNA (**Supplementary Table 5**). The *pks-1* and *nrps-1* promoters were inserted into the SalI/NotI

and AscI/NotI sites, respectively, of pPD114.108 or pPD114.108-*gfp::pest* to obtain *pks-1p::gfp* and *nrps-1p::gfp* or *pks-1p::gfp-pest* and *nrps-1p::gfp-pest*, respectively. For the *canp::mcherry* reporter, the CAN-specific promoter was cut from *canp::yfp*[24] (gift of Nadeem Moghal) at two SphI sites and inserted into pMC10 (a gift of Piali Sengupta). 50 ng/µL of the transgenes, along with 50 ng/µL of the co-injection marker *unc-122p::DsRed* (gift of Piali Sengupta), were injected into wild-type worms. At least three independent transgenic strains were analyzed. Imaging was conducted on a Zeiss Axiovert.A1 microscope equipped with ZEN lite 2012 camera.

Cyclic peptide 3 (2*S*,6*R*,10*R*,18*R*). ^{1}H NMR (600 MHz, dimethyl sulfoxide-d_6) δ 8.63 (brs, 10-NH), 8.20 (brd, $J_{6,6\text{-NH}}$ = 8.8 Hz, 6-NH), 7.80 (brs, 8-NH_2b), 7.49 (brd, $J_{2,2\text{-NH}}$ = 8.1 Hz, 2-NH), 7.43 (brs, 12-NH_2b), 7.36 (brs, 15-NH), 7.32 (brs, 8-NH_2a), 7.11 (brs, 4-NH_2b), 6.96 (brs, 12-NH_2a), 6.95 (brd, $J_{18,18\text{-NH}}$ = 7.9 Hz, 18-NH), 6.82 (brs, 4-NH_2a), 4.48 (m, H-2), 4.41 (m, H-6), 4.25 (m, H-10), 3.96 (m, H-18), 3.42 (m, H-15b), 3.18 (m, H-15a), 2.98 (dd, $J_{7a,7b}$ = 16.4 Hz, $J_{6,7b}$ = 4.7 Hz, H-7b), 2.62 (dd, $J_{3a,3b}$ = 19.3 Hz, $J_{2,3b}$ = 6.5 Hz, H-3b), 2.58 (brd, $J_{7a,7b}$ = 17.2 Hz, H-7a), 2.57 (overlap, H-14b), 2.51 (overlap, H-11a, 11b), 2.46 (overlap, H-17b), 2.43 (dd, $J_{3a,3b}$ = 19.4 Hz, $J_{2,3a}$ = 12.7 Hz, H-3a), 2.42 (overlap, H-14a), 2.15 (brd, $J_{17a,17b}$ = 12.0 Hz, H-17a), 0.98 (d, $J_{18,19}$ = 5.9 Hz, H-19); ^{13}C NMR (125 MHz, dimethyl sulfoxide-d_6) δ 173.6 (C-8, 12), 173.3 (C-13), 171.2 (C-4), 171.1 (C-9), 170.7 (C-16), 170.5 (C-5), 169.7 (C-1), 52.1 (C-10), 49.9 (C-2), 49.2 (C-6), 43.0 (C-18), 41.4 (C-17), 36.8 (C-3), 35.6 (C-11), 35.4 (C-7), 34.8 (C-15), 33.5 (C-14), 20.7 (C-19); ESIMS *m/z* 499.3 $[M+H]^+$, *m/z* 497.3 $[M-H]^-$.

Cyclic peptide 4 (2*R*,6*S*,10*R*,18*S*). ^{1}H NMR (600 MHz, dimethyl sulfoxide-d_6) δ 8.39 (brd, $J_{10,10\text{-NH}}$ = 7.4 Hz,10-NH), 7.92 (brs, 8-NH_2b), 7.85 (brd, $J_{2,2\text{-NH}}$ = 8.8 Hz, 2-NH), 7.81 (brd, $J_{6,6\text{-NH}}$ = 8.8

Hz, 6-NH), 7.47 (brs, 8-NH_2a), 7.38 (brs, 4-NH_2b), 7.33 (brs, 12-NH_2b), 7.25 (brs, 15-NH), 7.08 (overlap, 18-NH), 6.95 (brs, 12-NH_2a), 6.85 (brs, 4-NH_2a), 4.49 (m, H-2), 4.46 (m, H-10), 4.40 (m, H-6), 3.97 (m, H-18), 3.55 (overlap, H-15b), 3.14 (overlap, H-15a), 3.05 (dd, $J_{7a,7b}$ = 17.2 Hz, $J_{6,7b}$ = 3.8 Hz, H-7b), 2.69 (dd, $J_{3a,3b}$ = 15.8 Hz, $J_{2,3b}$ = 5.6 Hz, H-3b), 2.65 (dd, $J_{11a,11b}$ = 15.7 Hz, $J_{10,11b}$ = 6.8 Hz, H-11b), 2.54 (overlap, H-7a), 2.51 (overlap, H-17b), 2.48 (overlap, H-11a, 14b), 2.43 (dd, $J_{3a,3b}$ = 15.8 Hz, $J_{2,3a}$ = 6.9 Hz, H-3a), 2.36 (m, H-14a), 2.11 (brd, $J_{17a,17b}$ = 11.3 Hz, H-17a), 0.97 (d, $J_{18,19}$ = 5.9 Hz, H-19); ^{13}C NMR (125 MHz, dimethyl sulfoxide-d_6) δ 173.8 (C-8), 172.6 (C-13), 172.3 (C-12), 171.8 (C-4), 170.3 (C-5), 170.2 (C-9, 16), 169.6 (C-1), 49.7 (C-2), 49.3 (C-10), 48.7 (C-6), 43.1 (C-18), 41.5 (C-17), 35.4 (C-11), 35.3 (C-7), 35.1 (C-3), 34.7 (C-14), 34.3 (C-15), 20.9 (C-19); ESIMS *m/z* 499.3 $[M+H]^+$, *m/z* 497.2 $[M-H]^-$.

Cyclic peptide 5 (2*R*,6*R*,10*S*,18*S*). ^{1}H NMR (600 MHz, dimethyl sulfoxide-d_6) δ 8.89 (brd, $J_{6,6\text{-NH}}$ = 5.2 Hz, 6-NH), 8.48 (brs, 10-NH), 7.49 (brd, $J_{2,2\text{-NH}}$ = 7.9 Hz, 2-NH), 7.40 (brs, 12-NH_2b), 7.33 (brs, 8-NH_2b), 7.27 (brs, 4-NH_2b), 7.00 (brs, 15-NH), 6.98 (brs, 12-NH_2a), 6.89 (brs, 8-NH_2a), 6.88 (brs, 4-NH_2a), 6.66 (brd, $J_{18,18\text{-NH}}$ = 7.7 Hz, 18-NH), 4.40 (m, H-2, 10), 4.33 (m, H-6), 3.97 (m, H-18), 3.33 (overlap, H-15a,15b), 2.60 (overlap, H-7b), 2.56 (overlap, H-3a, 3b), 2.56 (overlap, H-14b), 2.49 (overlap, H-11b), 2.48 (overlap, H-7a), 2.36 (brd, $J_{17a,17b}$ = 13.1 Hz, H-17b), 2.31 (brd, $J_{11a,11b}$ = 16.1Hz, H-11a), 2.23 (m, H-14a), 2.06 (brd, $J_{17a,17b}$ = 13.0 Hz, $J_{17a,18}$ = 9.4 Hz, H-17a), 1.04 (d, $J_{18,19}$ = 6.5 Hz, H-19); ^{13}C NMR (125 MHz, dimethyl sulfoxide-d_6) δ 173.9 (C-9), 172.3 (C-13), 171.2 (C-4), 170.9 (C-8), 170.7 (C-5), 170.3 (C-12), 170.1 (C-1), 170.0 (C-16), 50.9 (C-2, 6, 10), 42.6 (C-18), 41.7 (C-17), 36.5 (C-3), 35.6 (C-11), 35.4 (C-7, 15), 34.0 (C-14), 20.1 (C-19); ESIMS *m/z* 499.3 $[M+H]^+$, *m/z* 497.3 $[M-H]^-$.

L1 recovery, dauer formation, and dauer recovery assays. For L1 recovery assays, eggs were isolated from well-fed gravid worms using alkaline bleach treatment, diluted to 4-6 eggs/ μL in M9 buffer, and shaken for 24 h at 22.5 °C and 225 rpm. Approximately 80-120 synchronized L1s were placed onto a 3 cm NGM plate with OP50 at 15 °C, 20 °C, or 25 °C. After a certain period of time (40 h at 25 °C, 48 h at 20 °C, and 80 h at 15 °C), the percentage of worms at or passed the L4 stage was determined. For each experiment, five plates were analyzed for each strain, the percentage of worms at or passed the L4 stage was calculated for each plate, and the percentages for each strain were averaged. Dauer formation assays were performed for wild-type, *pks-1*, and *nrps-1* with vehicle control or 1 μM asc-C6-MK at 25 °C as described[26]. Dauer recovery assays were performed by taking dauers from dauer formation assay plates and moving them to a lawn of bacteria for 24 h at 20 °C before scoring for recovery.

Egg to L4 development assay. Worms were maintained at 15 °C, 20 °C, or 25 °C for 2-3 generations. For egg lay assay, L4s were moved onto a new plate one day before the beginning of the experiment, and the next day 8 adults were used to perform a 1 h egg lay for each 3 cm NGM plate with OP50. Alternatively, for egg prep experiment, eggs were isolated from well-fed gravid worms using alkaline bleach treatment, washed, and added to 3 cm NGM plates with OP50. In both egg lay and egg prep assays, eggs were then incubated at 15 °C, 20 °C, or 25 °C, and after a certain period of time (40 h at 25 °C, 48 h at 20 °C and 80 h at 15 °C), the percentage of worms at or passed the L4 stage was determined. For each experiment, five plates were analyzed for each strain, and the percentages for each strain were averaged.

Analysis of expression of insulins using qRT-PCR. Well-fed gravid adults were collected from multiple 10 cm NGM plates and eggs were isolated by using alkaline bleach treatment, diluted to 4–6 eggs / µL in M9 buffer, and shaken for 24 h at 21 °C, 225 rpm. Then 25 mg/mL of OP50 was supplied to initiate recovery. Worms at 0 h and 6 h after feeding were collected by washing with cold M9 buffer, flash-frozen and stored at –80 °C before qRT-PCR. Total RNA extraction, an on-column DNase treatment, and cDNA generation were performed as described[26], except that 0.25 µg of total RNA was used for reverse transcription. All primers for insulin genes were as described[27], except for the ones for *ins-3*, *ins-26*, and *ins-31*, which were as described here[16], and the ones for *ins-11*, which were designed using the Real-time PCR Primer Design Tool (IDT) and are listed in **Supplementary Table 5**. qPCR was performed using SYBR Green select Master Mix (Life Technologies) on a 7500 Fast Real-Time PCR system (Applied Biosystems) using the standard mode. PCR parameters include a holding stage at 50 °C for 2 min and another holding stage at 95 °C for 5 min, followed by 40 cycles of 95 °C for 10s, 57 °C for 20s and 72 °C for 30s. Relative expression levels for recovered versus arrested L1s were determined using the $\Delta\Delta C_t$ method[28], and normalized to the expression levels of endogenous control genes *act-1*, *pmp-3* and Y45F10D.4[26]. Ratio of relative expression level for each strain was calculated by comparing the relative expression level at 6 h after feeding with the level at 0 h.

Nemamide production. Eggs were isolated from well-fed gravid worms using alkaline bleach treatment, diluted in S basal in a 125 mL flask, and shaken for 24 h at 20 °C and 200 rpm. Then, the synchronized L1s were inoculated into 2.8 L flasks with the density adjusted to 6 L1s / µL in 200 mL S medium (starved L1s) or 190 mL S medium plus 10 mL concentrated OP50 (fed L1s). Starved and fed L1 worms were cultured at 20 °C and 150 rpm for 6 h. L1s were then harvested

by washing three times with S basal. L1s were freeze-dried, ground with sand, and extracted with ethanol, as described above, and then the nemamides were analyzed by LC-MS.

M cell division assay. For the *ayIs7[hlh-8p::gfp], pks-1; ayIs7,* and *nrps-1; ayIs7* strains, eggs were isolated from well-fed gravid worms using alkaline bleach treatment, diluted to 4–6 eggs/ μL in M9 buffer with 0.08% ethanol, and shaken for 7d at 22.5 °C and 225 rpm. Worms were examined for M cell division using a fluorescent microscope. > 50 worms were examined for each genotype.

Fertility and brood size upon recovery from L1 arrest. For the wild-type, *pks-1*, and *nrps-1* strains, eggs were isolated from well-fed gravid worms using alkaline bleach treatment, diluted to 4–6 eggs/ μL in M9 buffer, and shaken for 5d at 22.5 °C and 225 rpm. Worms were then moved to a lawn of bacteria, allowed to develop to the L4 stage, and then singled. Survival and fertility were examined 2–3d later.

L1 survival assay. Eggs were isolated from well-fed gravid worms using alkaline bleach treatment, diluted in M9 buffer in a 125 mL flask, and shaken for 24 h at 20 °C and 200 rpm. Then, the density of the synchronized L1s was adjusted to 4-6 L1s / μL (**Fig. 2e**) or 20–25 L1s / μL (**Supplementary Fig. 24**, high density) or 0.5-0.8 L1s / μL (**Supplementary Fig. 24**, low density) in M9 buffer. Every other day, 20 μL starved L1 samples were seeded onto 3 cm NGM plate with OP50 at 20 °C, and three plates were seeded for each strain. The plated worms were scored after 2–3 d, and worms at or passed the L2 stage were scored as surviving worms. For each experiment, three plates were analyzed for each strain, the percentage of surviving worms was calculated for

each plate, and the percentages for each strain were averaged. Survival curves in **Figure 2e** and **Supplementary Figure 24** and **Supplementary Figure 27** were statistically analyzed as previously described[29].

Pumping assay. At least 30 young adults for each strain (wild-type, *pks-1*, and *nrps-1*) were analyzed while on a lawn of OP50 by counting the number of pharynx pumps per 30s under the dissecting microscope at room temperature.

Phylogeny and domain analysis. Phylogenetic trees were generated in MEGA 6, and domain analysis was performed using antiSMASH 3.0.[30,31] Protein sequences were retrieved from NCBI or Wormbase Parasite.

References

22 Ramaswamy, V. *et al.* Development of a ^{13}C-optimized 1.5-mm high temperature superconducting NMR probe. *J. Magn. Reson.* **235**, 58-65 (2013).

23 Chambers, M. C. *et al.* A cross-platform toolkit for mass spectrometry and proteomics. *Nat. Biotechnol.* **30**, 918-920 (2012).

24 Butcher, R. A., Fujita, M., Schroeder, F. C. & Clardy, J. Small-molecule pheromones that control dauer development in *Caenorhabditis elegans*. *Nat. Chem. Biol.* **3**, 420-422 (2007).

25 Modzelewska, K., Lauritzen, A., Hasenoeder, S., Brown, L., Georgiou, J. & Moghal, N. Neurons refine the *Caenorhabditis elegans* body plan by directing axial patterning by Wnts. *PLoS Biol.* **11**, e1001465 (2013).

26 Zhang, X. *et al.* Acyl-CoA oxidase complexes control the chemical message produced by *Caenorhabditis elegans*. *Proc. Natl. Acad. Sci. U. S. A.* **112**, 3955-3960 (2015).

27 Ritter, A. D. *et al.* Complex expression dynamics and robustness in *C. elegans* insulin networks. *Genome Res.* **23**, 954-965 (2013).

28 Livak, K. J. & Schmittgen, T. D. Analysis of relative gene expression data using real-time quantitative PCR and the $2^{-\Delta\Delta C_T}$ Method. *Methods* **25**, 402-408 (2001).

29 Zhang, X., Zabinsky, R., Teng, Y., Cui, M. & Han, M. microRNAs play critical roles in the survival and recovery of *Caenorhabditis elegans* from starvation-induced L1 diapause. *Proc. Natl. Acad. Sci. U. S. A.* **108**, 17997-18002 (2011).

30 Tamura, K., Stecher, G., Peterson, D., Filipski, A. & Kumar, S. MEGA6: Molecular Evolutionary Genetics Analysis version 6.0. *Mol. Biol. Evol.* **30**, 2725-2729 (2013).
31 Weber, T. *et al.* antiSMASH 3.0-a comprehensive resource for the genome mining of biosynthetic gene clusters. *Nucleic Acids Res.* **43**, W237-243 (2015).

Supplementary Information

A hybrid polyketide-nonribosomal peptide in nematodes that promotes larval survival

Qingyao Shou†, Likui Feng†, Yaoling Long, Jungsoo Han, Joshawna K. Nunnery, David H. Powell, Rebecca A. Butcher*

Department of Chemistry, University of Florida, Gainesville, FL 32611

†equal contributions
*Correspondence to: butcher@chem.ufl.edu

This PDF file includes:

Supplementary Figures 1-28
Supplementary Tables 1-5

Supplementary Results

Table of Contents

Contents	**Page**
Supplementary Figure 1. Phylogeny and domain analysis of PKS-1 and NRPS-1 homologs	3
Supplementary Figure 2. Extracted ion chromatograms	5
Supplementary Figure 3. NMR spectra for nemamide A	6
Supplementary Figure 4. Key dqf-COSY, HMBC, and ROESY correlations	15
Supplementary Figure 5. Relative configuration at C-2 and C-18	16
Supplementary Figure 6. Relative configuration at C-18 and C-20	16
Supplementary Figure 7. Relative configuration at C-20 and C-22	17
Supplementary Figure 8. Chemical structures of the model cyclic peptides	18
Supplementary Figure 9. Predicted and observed CD spectra for nemamide A	19
Supplementary Figure 10. In-source CID of nemamide A and B	20
Supplementary Figure 11. LC-MS data for in-source CID of nemamide A and B	21
Supplementary Figure 12. NMR spectra for nemamide B	22
Supplementary Figure 13. Alignment of PKS-1 KR domains	26
Supplementary Figure 14. Alignment of PKS-1 and NRPS-1 TE domains	27
Supplementary Figure 15. Phylogeny of PKS-1 and NRPS-1 TE domains	28
Supplementary Figure 16. Comparison of development of wild-type, *pks-1*, and *nrps-1* worms	29
Supplementary Figure 17. Dauer formation and recovery in wild-type, *pks-1*, and *nrps-1* worms	30
Supplementary Figure 18. M-cell imaging of wild-type, *pks-1*, and *nrps-1* worms	31
Supplementary Figure 19. Fertility and brood size of wild-type, *pks-1*, and *nrps-1* worms	32
Supplementary Figure 20. Expression of insulins in arrested L1s	33
Supplementary Figure 21. Expression of insulins in recovered versus arrested L1s	35
Supplementary Figure 22. Nemamide production in arrested and recovered L1s	37
Supplementary Figure 23. L1 survival in different mutant backgrounds	38
Supplementary Figure 24. L1 survival at low and high population densities	39
Supplementary Figure 25. Feeding rate of wild-type, *pks-1*, and *nrps-1* worms	40
Supplementary Figure 26. Pharynx pumping rate of wild-type, *pks-1*, and *nrps-1* worms	41
Supplementary Figure 27. Effect of an *unc-31* null mutation on survival of arrested L1s	42
Supplementary Figure 28. Model for the role of the nemamides in L1 arrest and survival	43
Supplementary Table 1. NMR data for nemamide A	44
Supplementary Table 2. NMR data for cyclic peptides	45
Supplementary Table 3. Comparison of the cyclic peptides and nemamide A	46
Supplementary Table 4. Comparison of A domain selectivity codes	47
Supplementary Table 5. Primer sequences	48

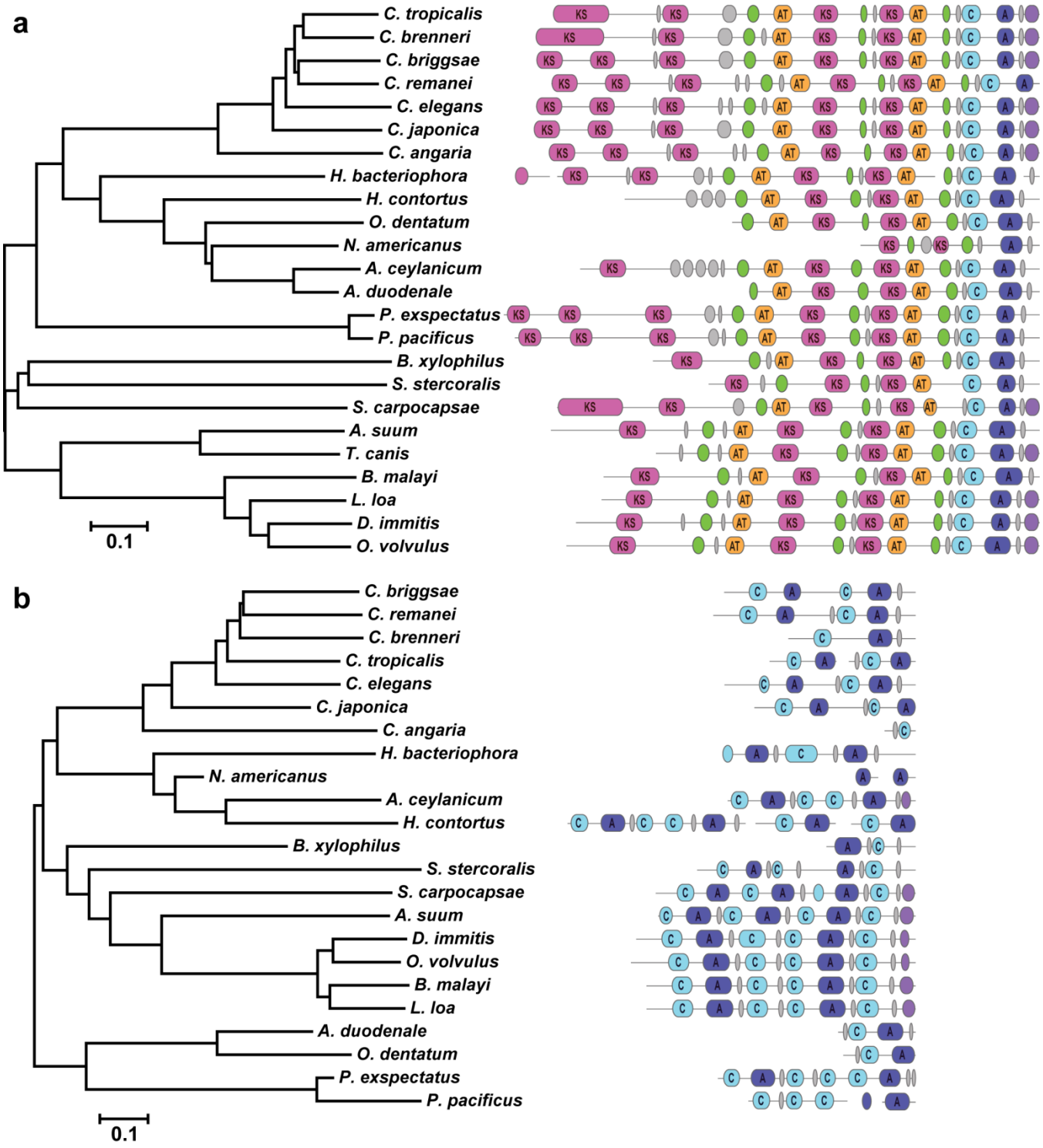

Supplementary Figure 1. Phylogeny and domain analysis of PKS-1 and NRPS-1 homologs. Phylogeny and protein domain analysis was performed as described in the methods for PKS-1 homologs (**a**) and NRPS-1 homologs (**b**) in the following nematode species: *Ancylostoma ceylanicum* (**a**, EYC37444.1; **b**, EYB85901.1), *Ancylostoma duodenale* (**a**, KIH69030.1; **b**, KIH67424.1), *Ascaris suum* (**a**, PRJNA80881; **b**, GS_05892), *Brugia malayi* (**a**, CDQ05007.1; **b**, XP_001901640.1), *Bursaphelenchus xylophilus* (**a**, BUX.s00713.159; **b**, BUX.gene.s01513.336), *Caenorhabditis angaria* (**a**, Cang_2012_03_13_00116.g4813; **b**, Cang_2012_03_13_00228.g7416), *C. brenneri* (**a**,

EGT30644.1; **b**, EGT46479.1), *C. briggsae* (**a**, EGT30644.1; **b**, CAP32083.2), *C. elegans* (**a**, NP_508923.2; **b**, CAC70135.3), *C. japonica* (**a**, CJA00126; **b**, CJA13923), *C. remanei* (**a**, XP_003118401.1; **b**, EFP02416.1), *C. tropicalis* (**a**, Csp11.Scaffold626.g6628; **b**, Csp11.Scaffold488.g2019), *Dirofilaria immitis* (**a**, nDi.2.2.2.g06619; **b**, nDi.2.2.2.g03539), *Haemonchus contortus* (**a**, CDJ83277.1; **b**, CDJ93083.1, CDJ93084.1, CDJ82649.1), *Heterorhabditis bacteriophora* (**a**, ACKM01001433.1; **b**, Hba_08702), *Loa Loa* (**a**, EJD75257.1; **b**, EFO26749.2), *Necator americanus* (**a**, ETN74557.1; **b**, NECAME_19208, NECAME_19210), *Oesophagostomum dentatum* (**a**, KHJ99846.1; **b**, KHJ98077.1), *Onchocerca volvulus* (**a**, OVOC1839; **b**, OVOC7029), *Pristionchus exspectatus* (**a**, scaffold450-EXSNAP2012.7; **b**, scaffold1344-EXSNAP2012.3), *P. pacificus* (**a**, PPA23686; **b**, PPA07616, PPA07617, PPA31783), *Steinernema carpocapsae* (**a**, L596_g18665.t1; **b**, L596_g20331.t1), *Strongyloides stercoralis* (**a**, SSTP_0001127100.1; **b**, SSTP_0000446000.1), *Toxocara canis* (**a**, KHN84567.1). If available, the Genbank accession number for the protein is listed, or, if not available, the protein name from Wormbase Parasite is listed. If a given species contained multiple proteins with homology to *pks-1* and/or *nrps-1*, the domains were annotated for all of the proteins using antiSMASH[1], but only the longest protein was used for generation of the phylogenetic tree. For the *H. bacteriophora pks-1* homolog, DNA sequence rather than protein sequence was analyzed (by first converting it to protein sequence using antiSMASH[1]). Domains depicted include ketosynthase (KS, pink), acyl carrier protein (ACP, grey), ketoreductase (KR, green), acyl transferase (AT, yellow), peptidyl carrier protein (PCP, grey), condensation (C, light blue), adenylation (A, dark purple), thioesterase (TE, light purple).

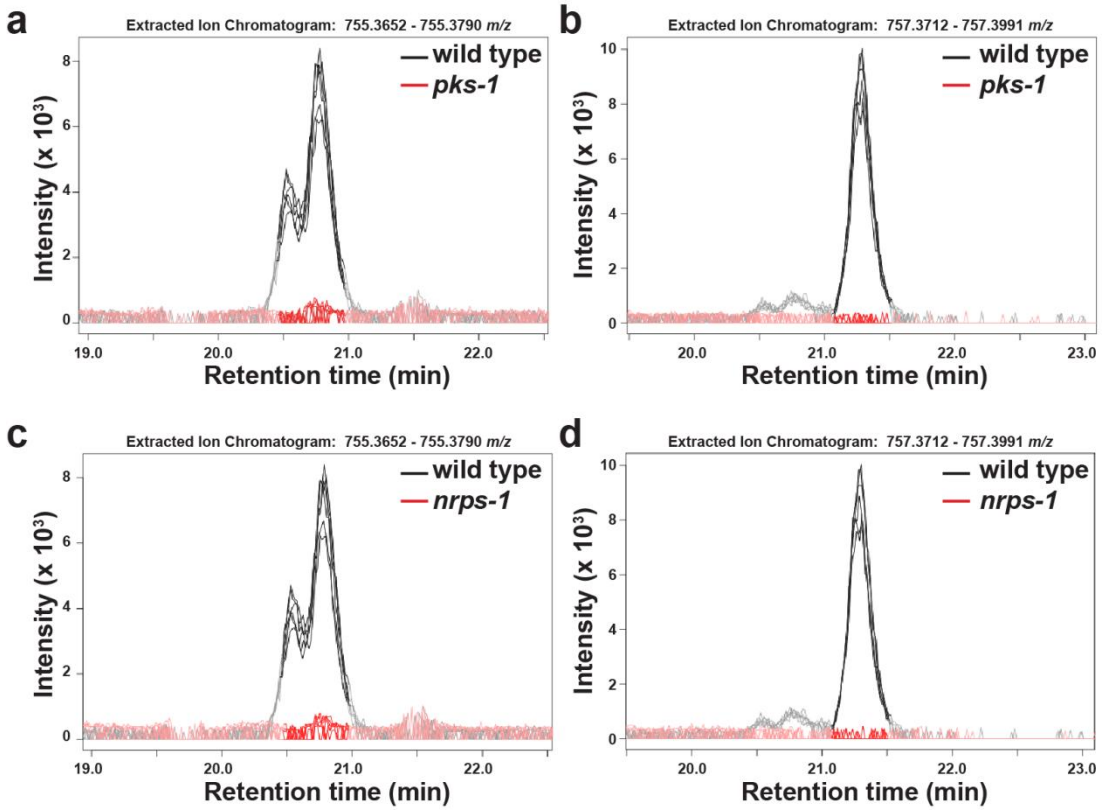

Supplementary Figure 2. Extracted ion chromatograms. Extracted ion chromatograms for *m/z* 755 (**a**,**c**) and *m/z* 757 (**b**,**d**) in wild-type versus *pks-1* mutant samples (**a**,**b**) and in wild-type versus *nrps-1* mutant samples (**c**,**d**). The *m/z* 755 feature always appears as one major and one minor peak, likely indicating two isomers. Images were generated in XCMS.[2]

Supplementary Figure 3. NMR spectra for nemamide A in dimethyl sulfoxide-d_6.
(**a**) ^{1}H NMR spectrum (with water suppression, contaminant peaks are indicated with asterisks).

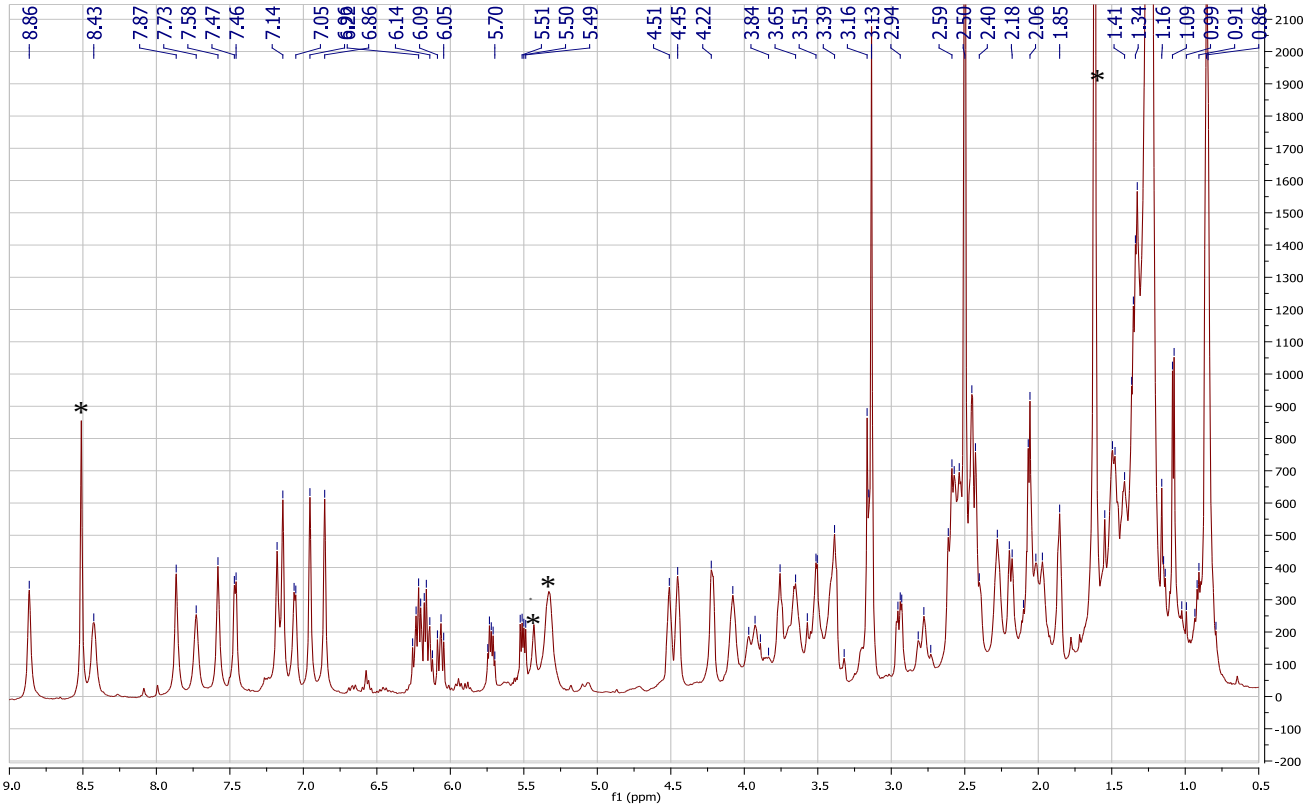

(**b**) ^{1}H NMR spectrum (without water suppression, contaminant peaks are indicated with asterisks).

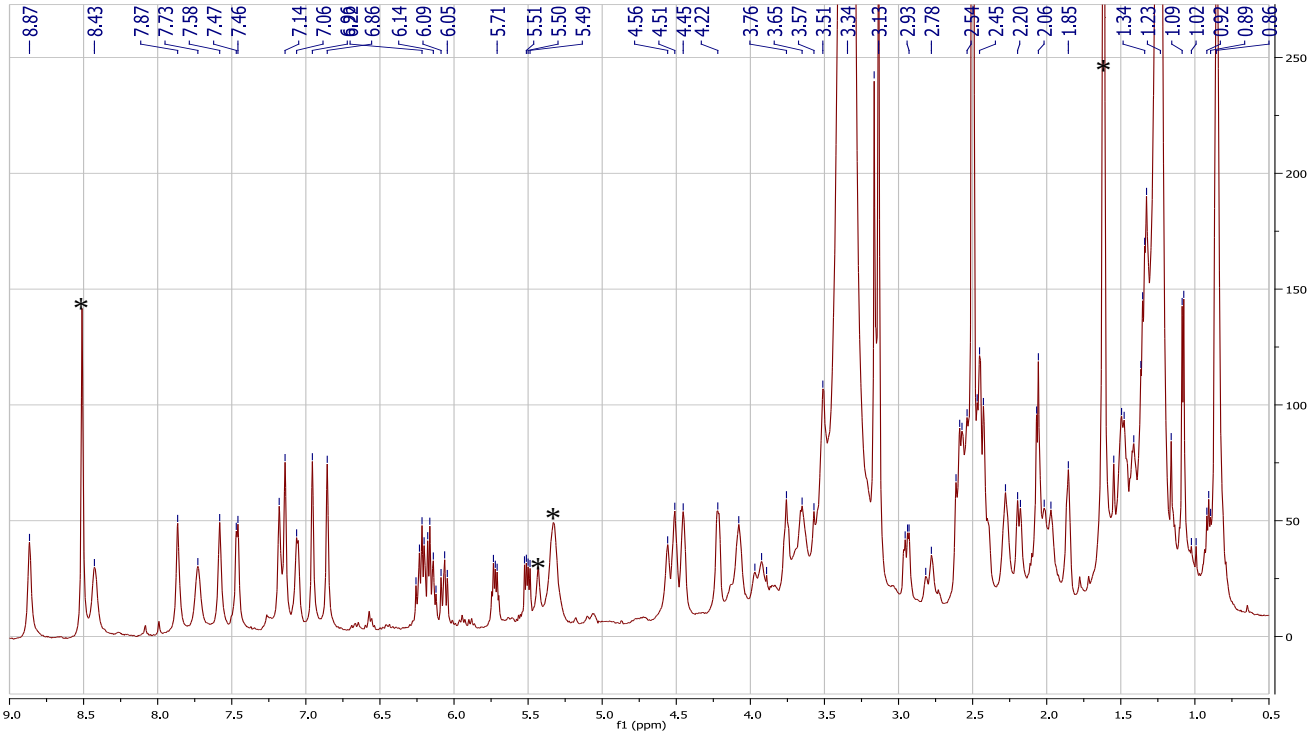

(**c**) dqf-COSY spectrum.

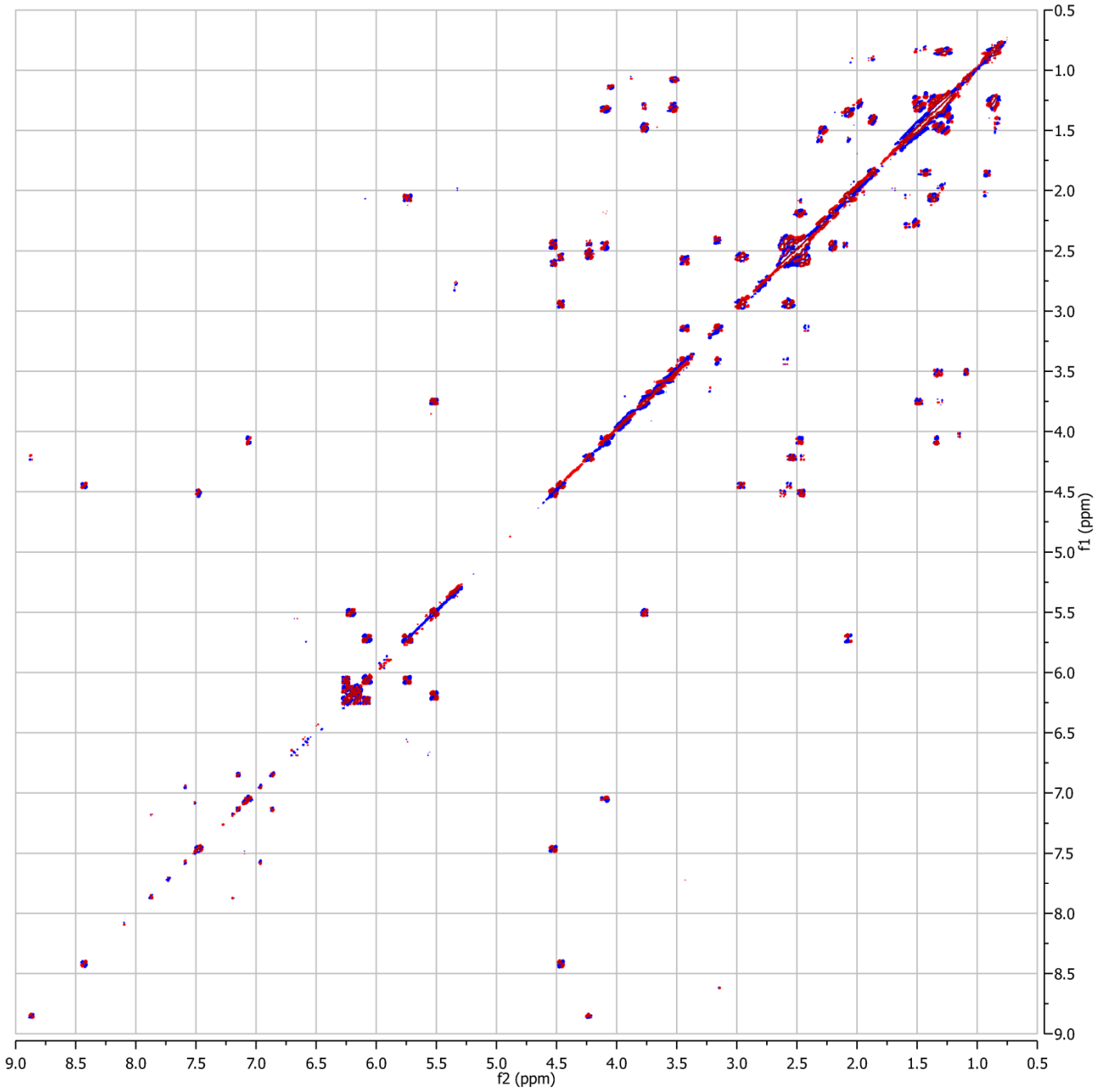

(**d**) dqf-COSY spectrum (0.5-5ppm region).

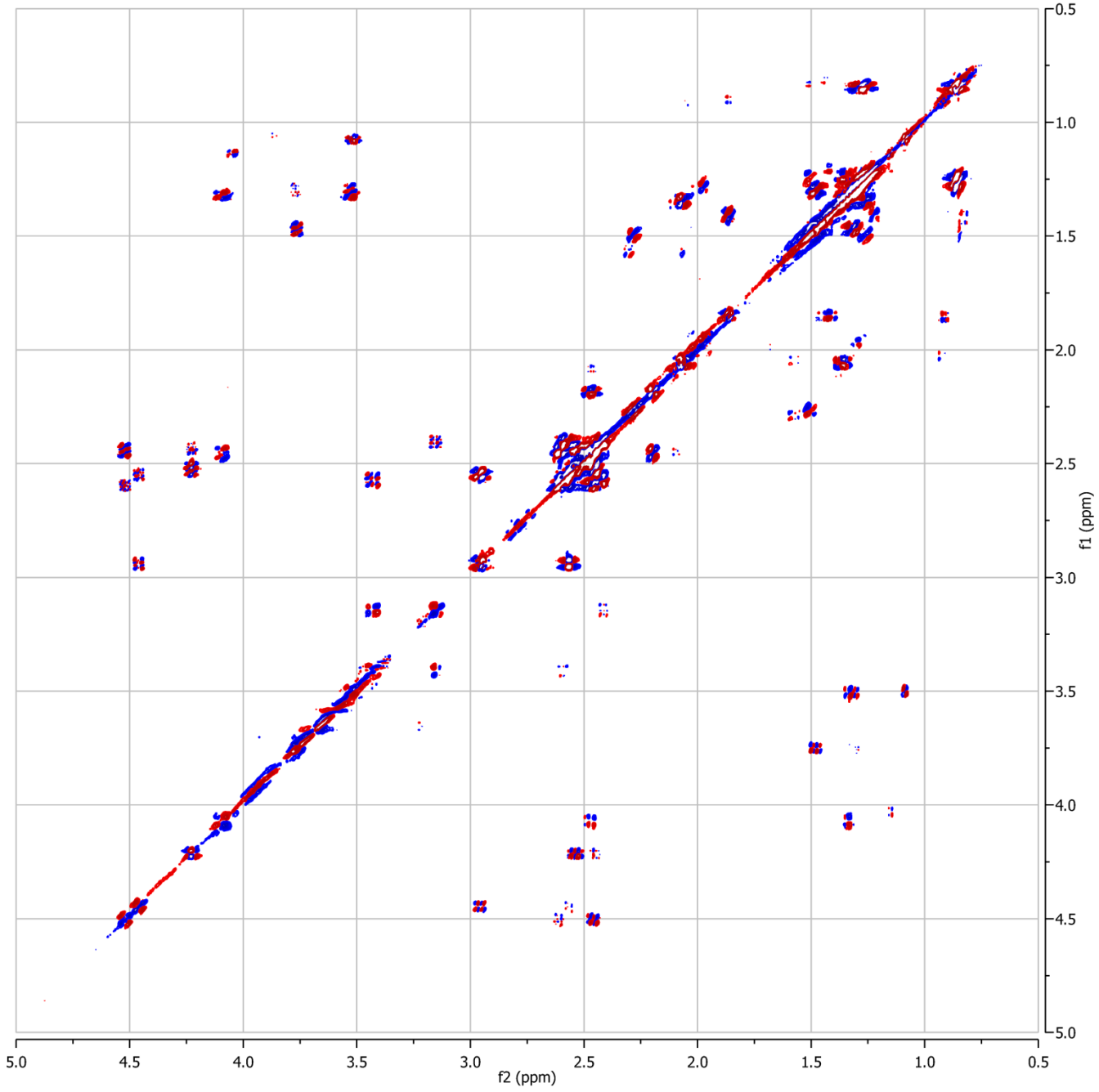

(**e**) TOCSY spectrum.

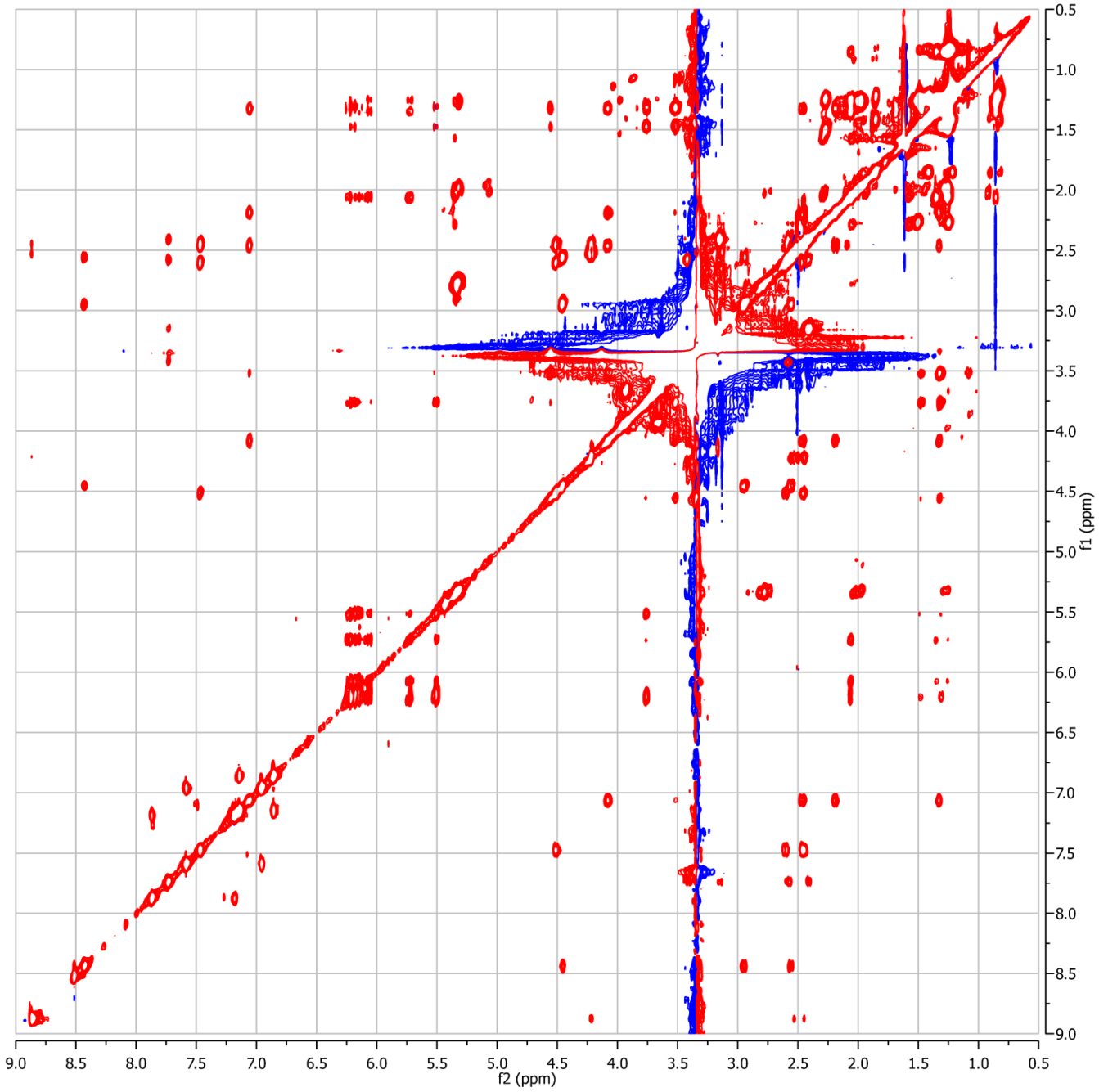

(**f**) HSQC spectrum.

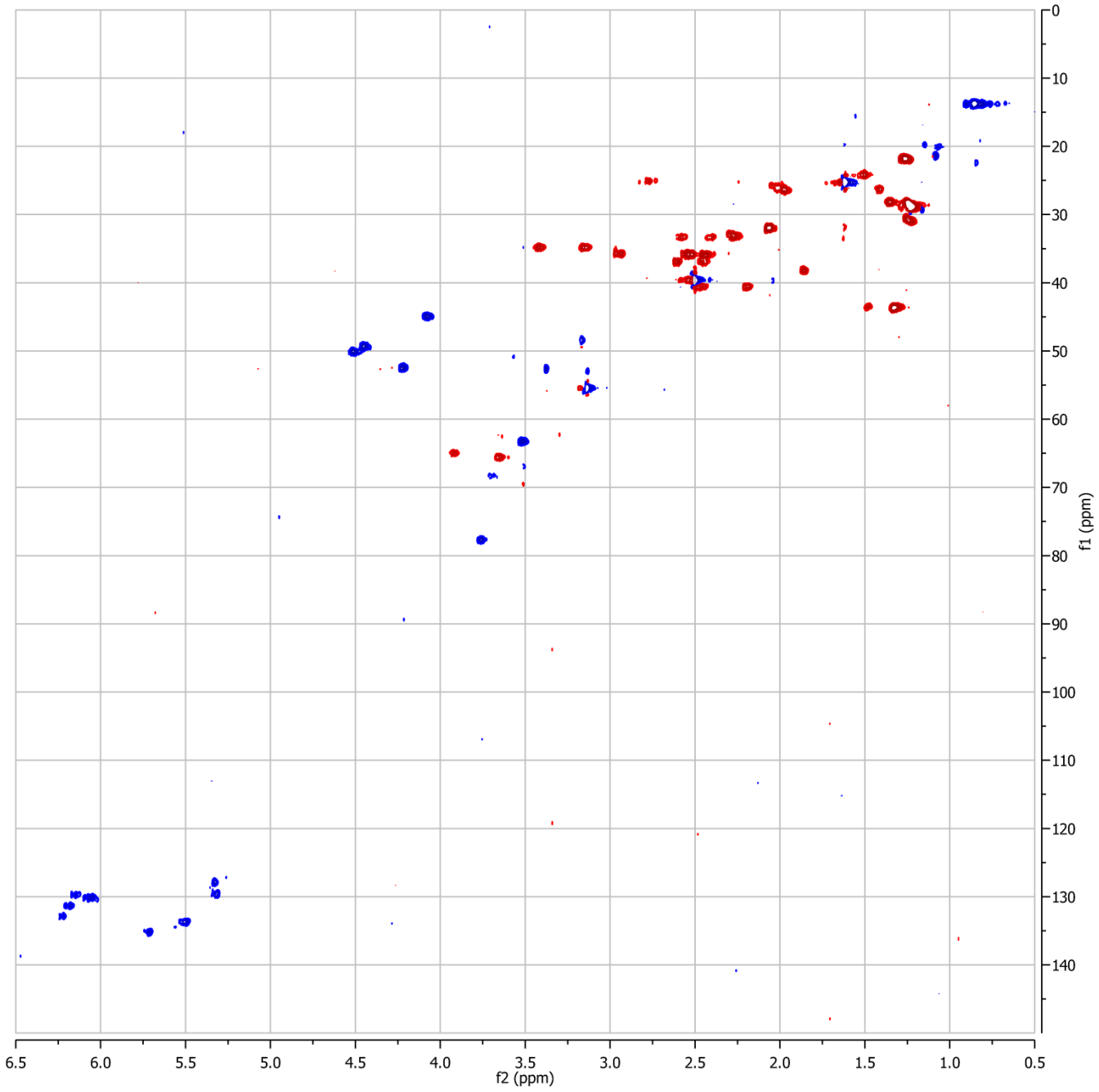

(**g**) HSQC spectrum (0.5-5ppm region).

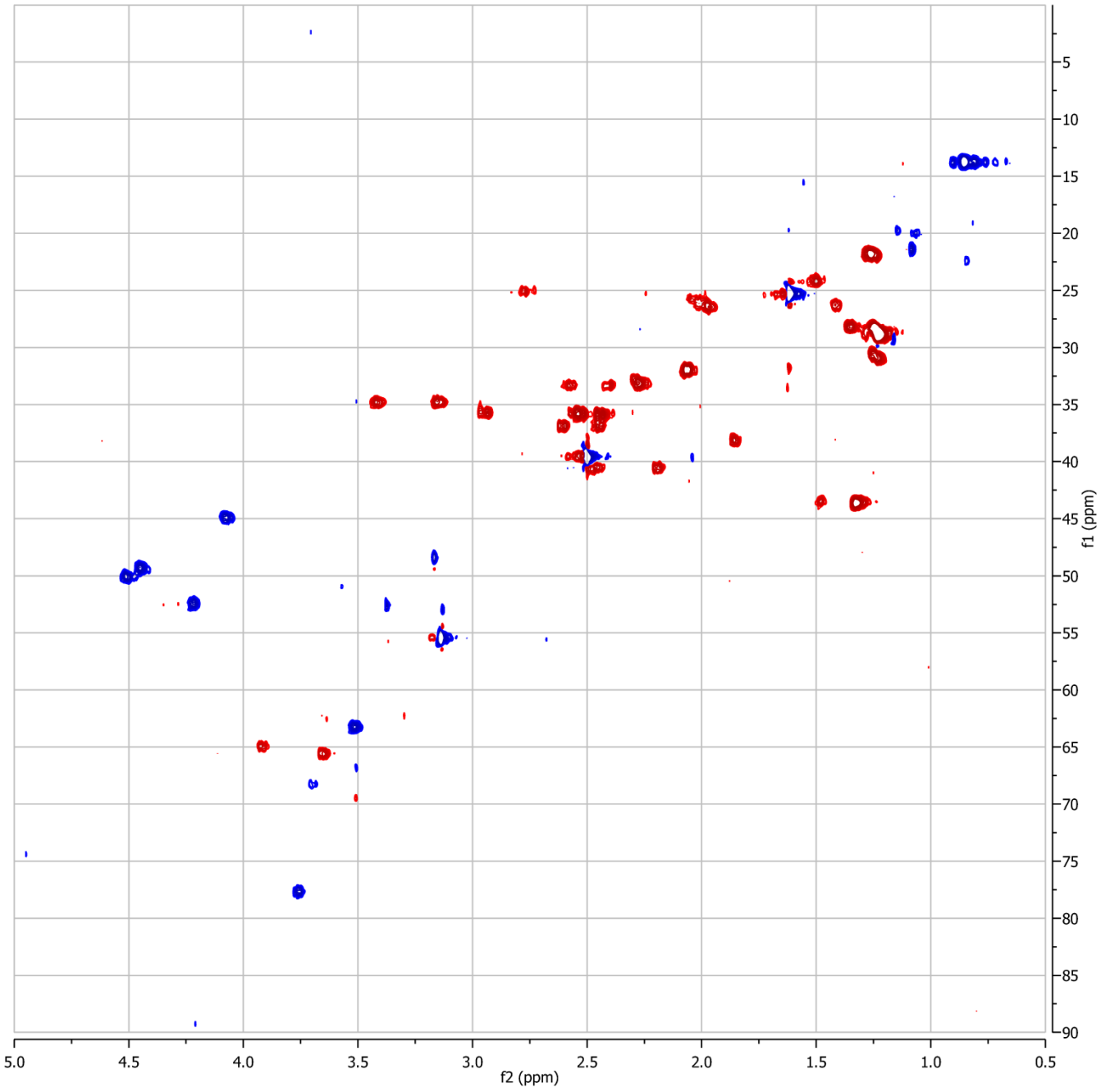

(**h**) HMBC spectrum.

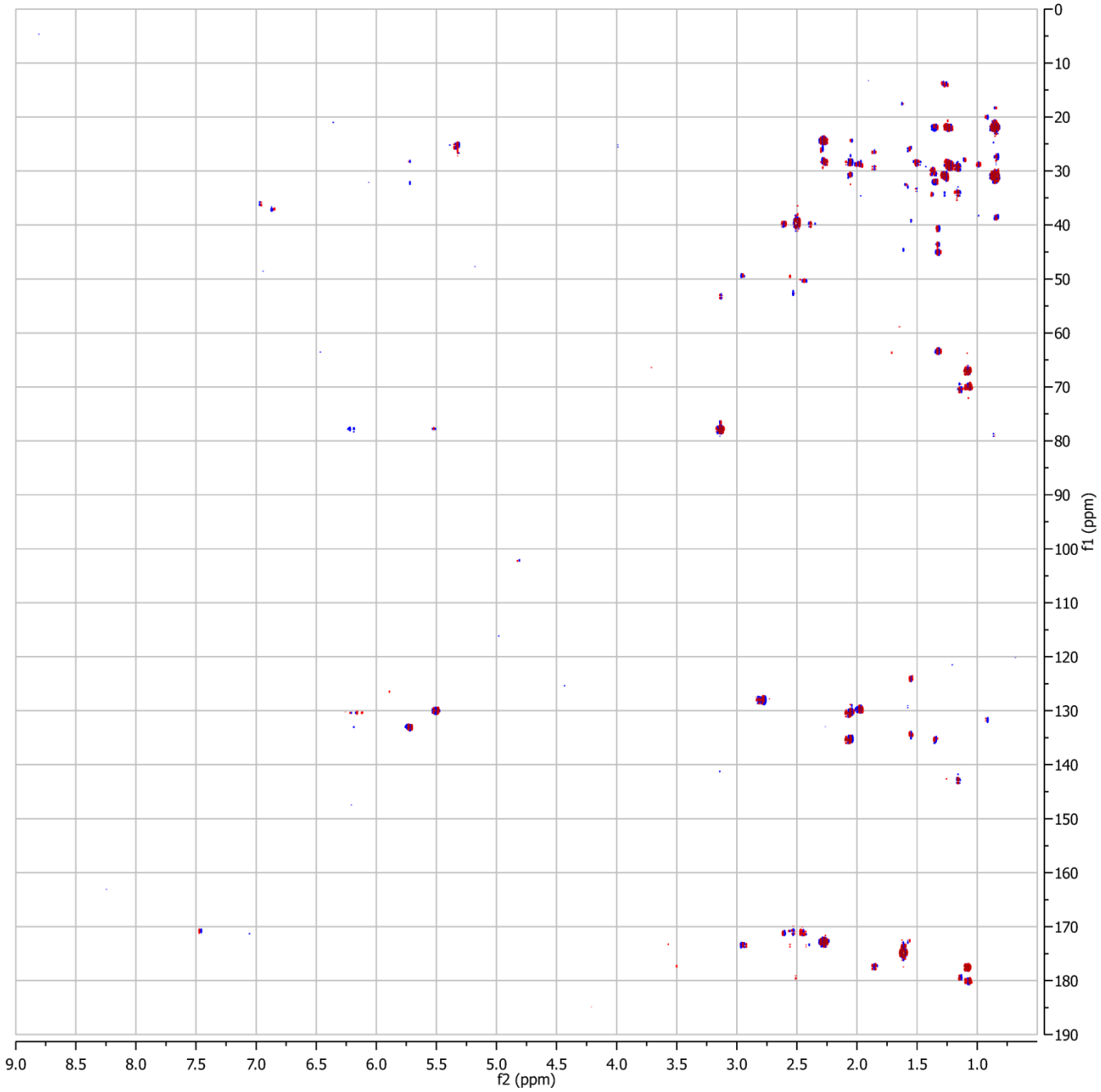

(**i**) HMBC spectrum obtained on a Bruker Avance 800 MHz NMR spectrometer.

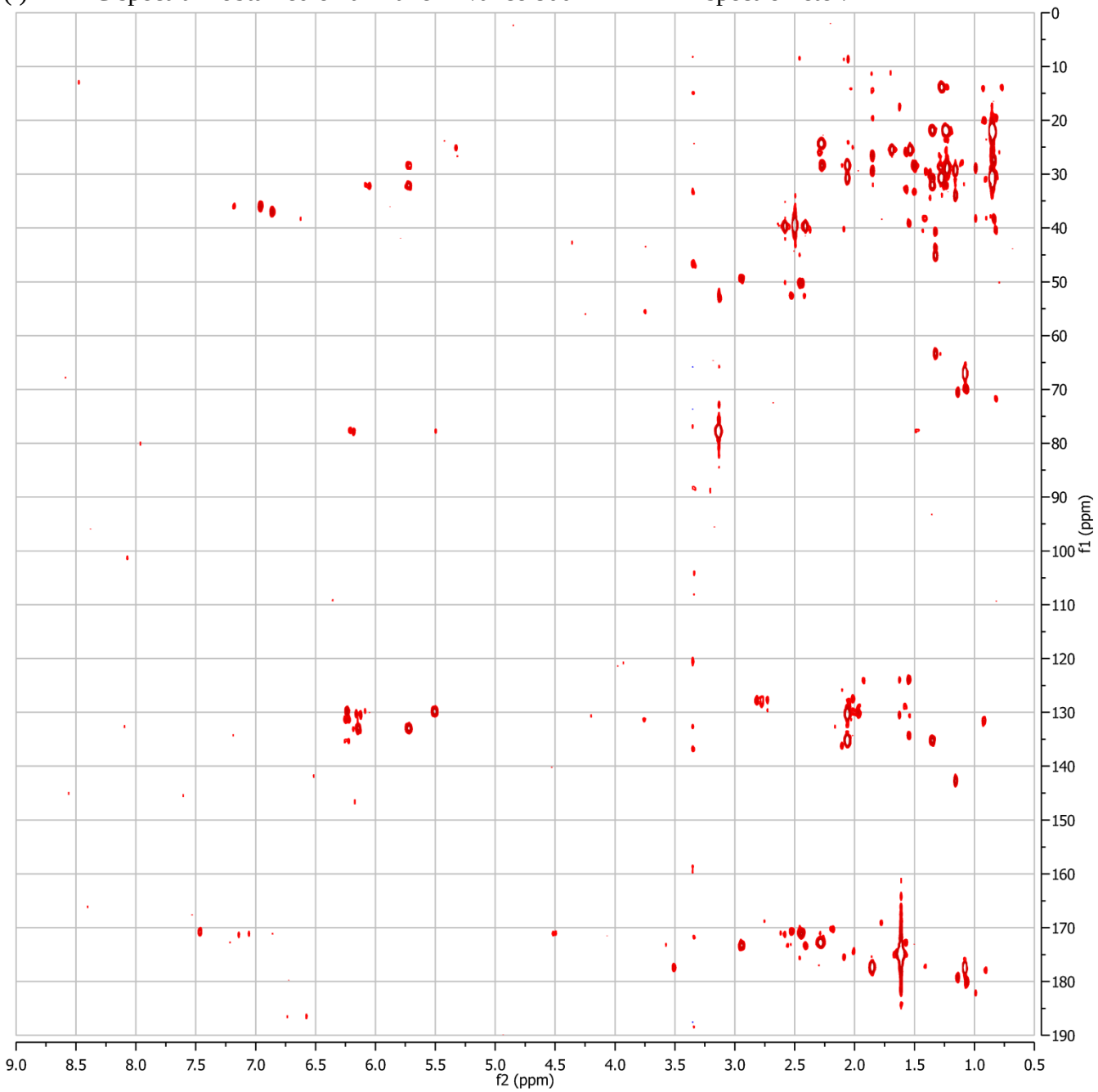

(**j**) ROESY spectrum.

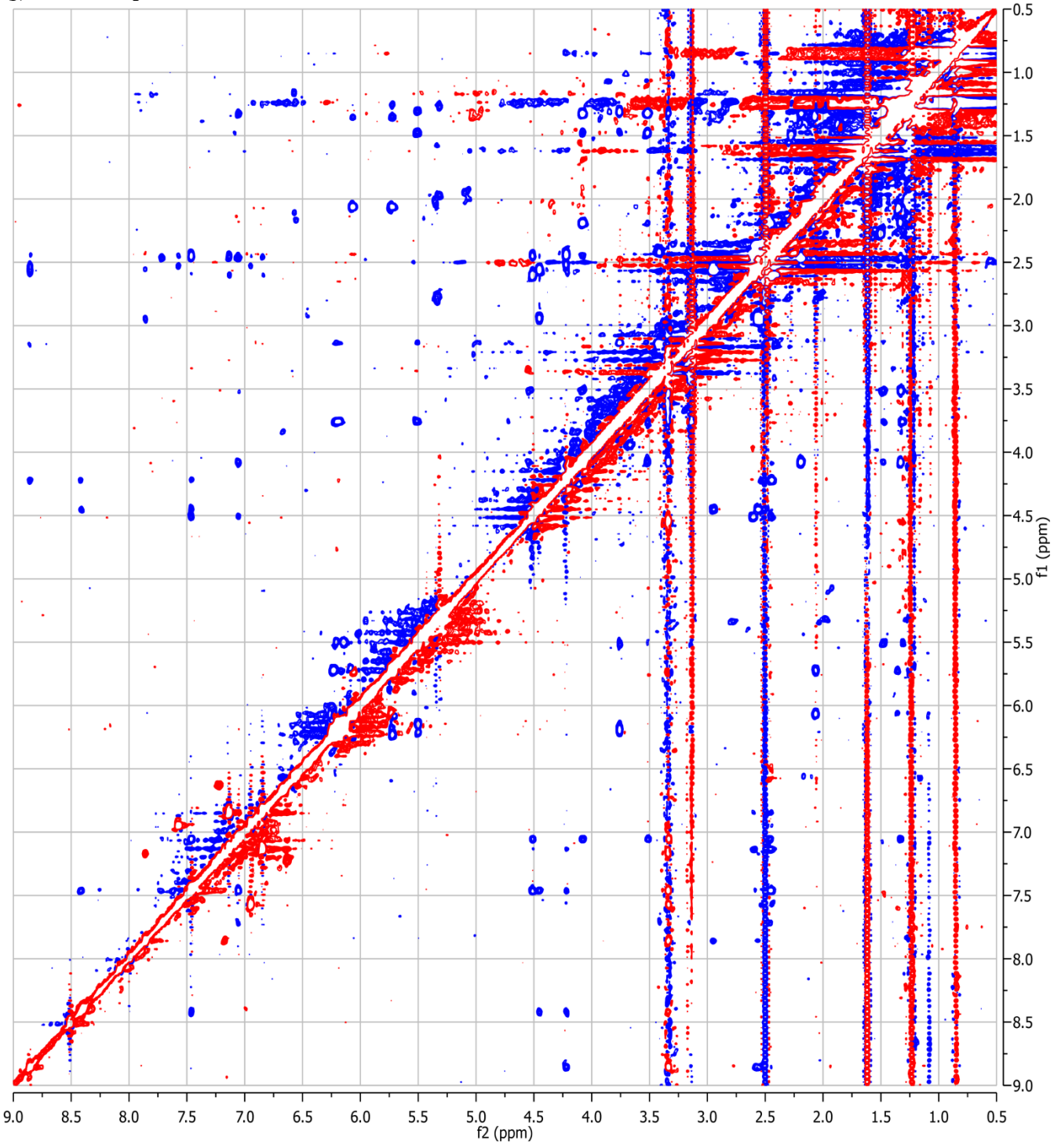

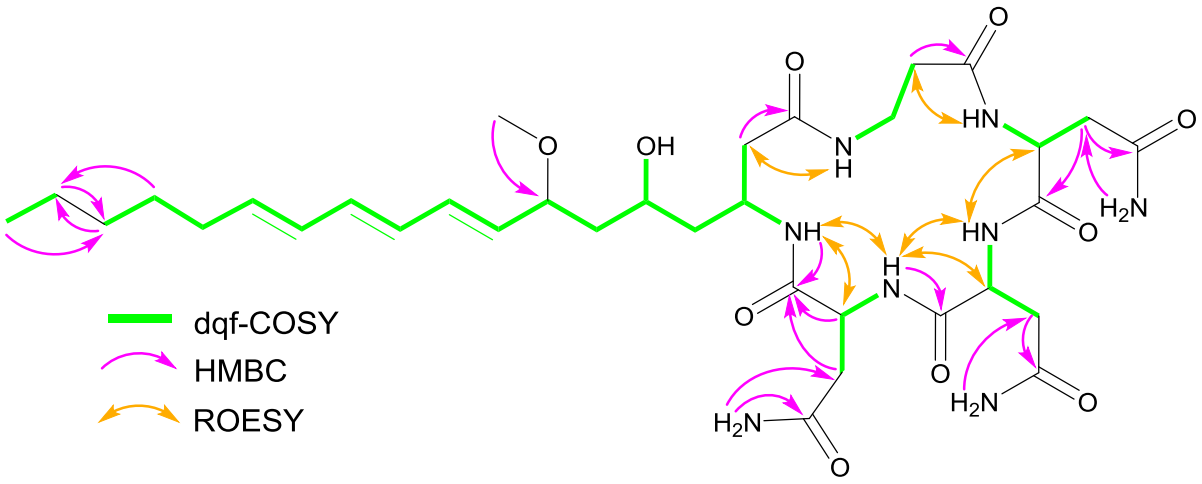

Supplementary Figure 4. Key dqf-COSY, HMBC, and ROESY correlations used to establish the molecular connectivity of nemamide A.

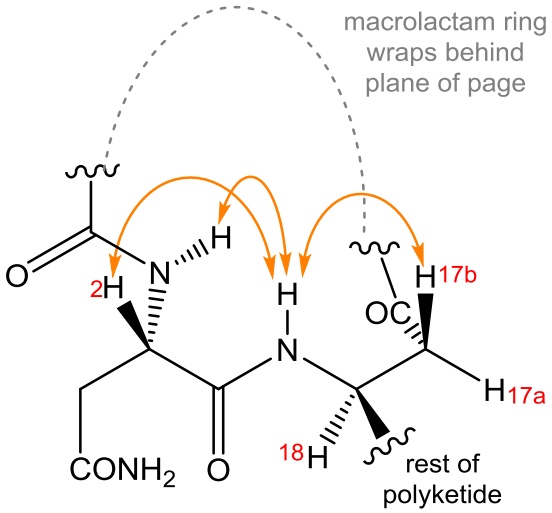

Supplementary Figure 5. Relative configuration of the stereocenters at C-2 and C-18. Nemamide A must have the absolute configuration shown (2*S*,18*R*) or the opposite absolute configuration (2*R*,18*S*) based on key ROESY correlations (indicated with orange double-headed arrows). The conformation depicted accounts for the weak *J* coupling between H-17a and 18 and the strong *J* coupling between H-17b and 18.

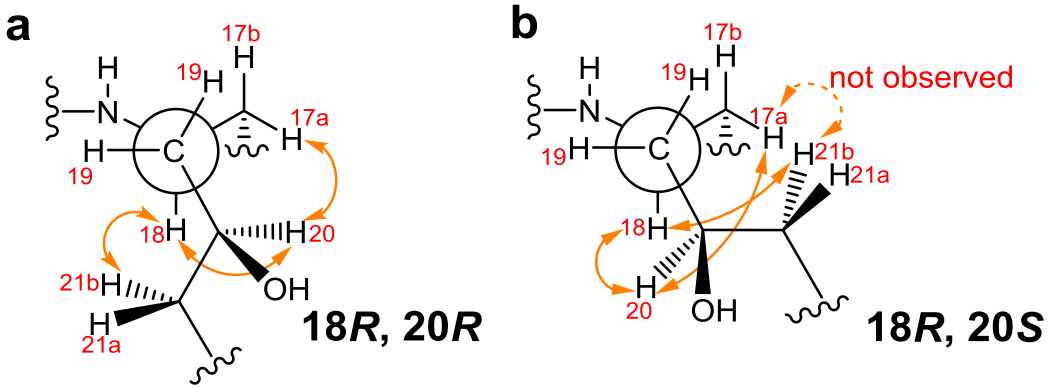

Supplementary Figure 6. Relative configuration of the stereocenters at C-18 and C-20. (**a**) Nemamide A has the absolute configuration shown (18*R*,20*R*) or the opposite absolute configuration (18*S*,20*S*) based on key ROESY correlations (indicated with orange double-headed arrows). The depicted conformation accounts for the weak *J* coupling between H-20 and H-21b and the strong *J* coupling between H-20 and H-21a. (**b**) The absolute configuration shown (18*R*,20*S*) or the opposite absolute configuration (18*S*,20*R*) is unlikely given the relative strength of the three ROESY correlations shown, as well as the fact that no correlation between H-17a and H-21b is observed in the ROESY spectrum.

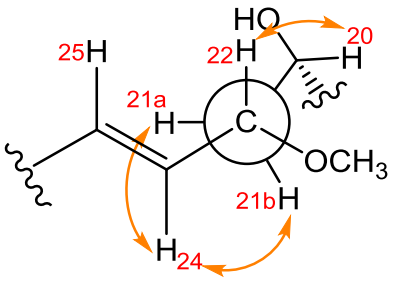

Supplementary Figure 7. Relative configuration of the stereocenters at C-20 and C-22. Nemamide A must have the absolute configuration shown (20*R*,22*S*) or the opposite absolute configuration (20*S*,22*R*) based on key ROESY correlations (indicated with orange double-headed arrows). The depicted conformation accounts for the weak *J* coupling between H-20 and H-21b and the strong *J* coupling between H-20 and H-21a. It also accounts for the weak *J* coupling between H-21a and H-22 and the strong *J* coupling between H-21b and H-22.

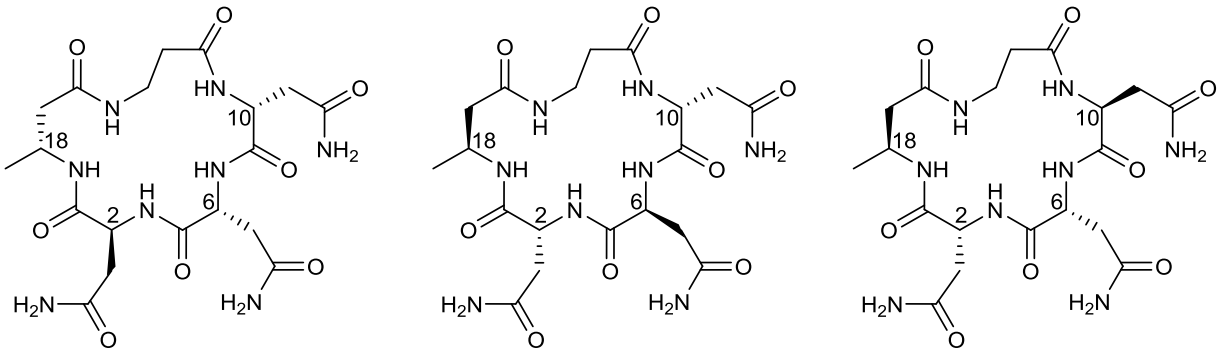

cyclic peptide **3** (2*S*,6*R*,10*R*,18*R*)

cyclic peptide **4** (2*R*,6*S*,10*R*,18*S*)

cyclic peptide **5** (2*R*,6*R*,10*S*,18*S*)

Supplementary Figure 8. Chemical structures of the model cyclic peptides that were synthesized in order to determine the absolute configurations of C-2, C-6, C-10, and C-18 in nemamide A. There are three possible positions for the L-Asn in the macrolactam ring of nemamide A, leading to the configurations 2*S*,6*R*,10*R*, 2*R*,6*S*,10*R*, and 2*R*,6*R*,10*S*. The relative configuration of the stereocenter at C-18 can be determined relative to the configuration of the most C-terminal Asn (that is, the configuration of the stereocenter at C-2), based on key ROESY correlations (Supplementary Fig. 5). Therefore, there are three possible absolute configurations for the four stereocenters in the macrolactam ring of nemamide A. Model cyclic peptides in which the polyketide tail of nemamide A was truncated as a methyl group were synthesized with the three possible absolute configurations of the four stereocenters: cyclic peptide **3** (2*S*,6*R*,10*R*,18*R*), cyclic peptide **4** (2*R*,6*S*,10*R*,18*S*), and cyclic peptide **5** (2*R*,6*R*,10*S*,18*S*).

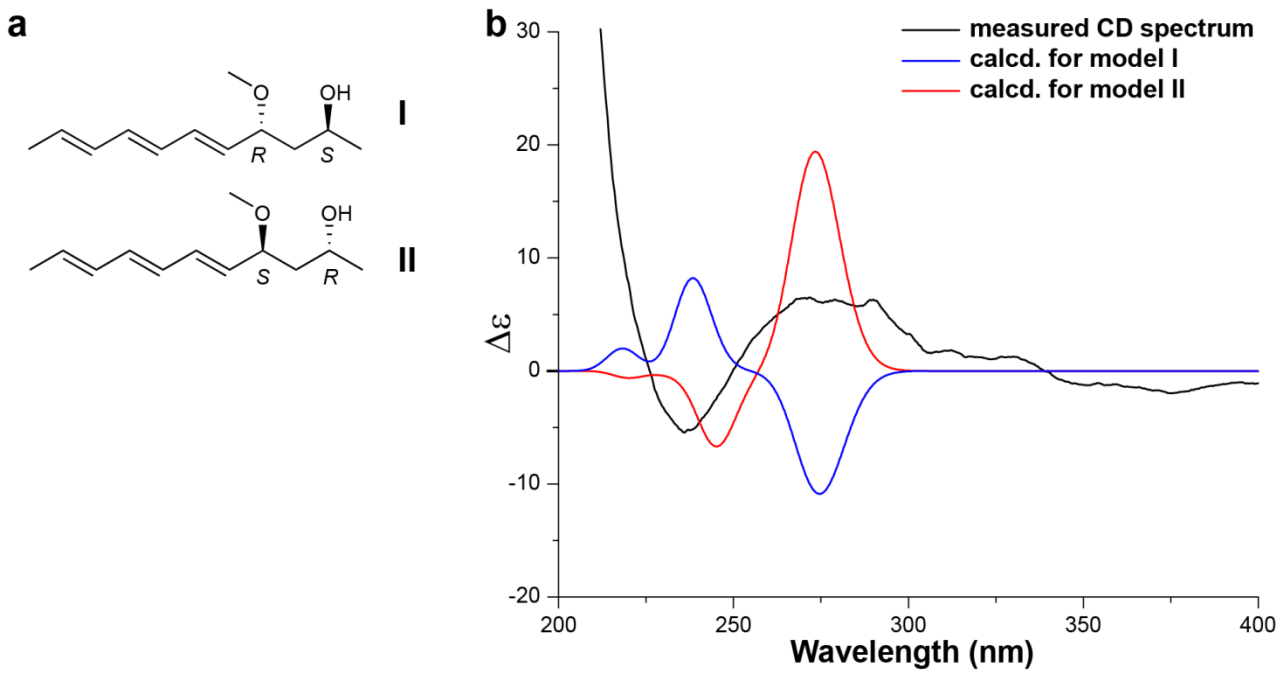

Supplementary Figure 9. Predicted and observed CD spectra of nemamide A. (**a**) Structures of model compounds I and II that were used to generate calculated CD spectra. In nemamide A, the configuration of the stereocenter at C-22 can be determined relative to the configuration of the stereocenter at C-20, based on key ROESY correlations (Supplementary Fig. 7). Thus, nemamide A is either 20*R*,22*S* or 20*S*,22*R*. The Cotton effects in the CD spectrum of nemamide A are predicted to depend largely on the configuration of the stereocenter nearest to the triene chromaphore (C-22). Thus, comparison of the calculated CD spectra of model compounds I and II to the CD spectrum of nemamide A should provide further confirmation of the absolute configuration of C-22 (and therefore C-20) in nemamide A.[3,4] (**b**) CD spectrum of nemamide A obtained in methanol, as well as calculated CD spectra of model compounds I (corresponding to nemamide A with 20*S*,22*R* configuration) and II (corresponding to nemamide A with 20*R*,22*S* configuration), suggesting that nemamide A has the 20*R*,22*S* configuration. The CD spectrum of nemamide A is weak because the compound has limited solubility in methanol and only dissolves well in dimethyl sulfoxide, which is not compatible with CD spectroscopy (of nemamide A). For calculating the CD spectra of the model compounds, the low energy conformations of the compounds were first calculated using Sybyl-X 2.1. Specifically, the random search algorithm was performed (100 cycles with an energy cutoff of 3.0 kcal/mol) while enforcing the constraints that the dihedral angles between "H-20" and "H-21a" and between "H-21b" and "H-22" should be 180° and that the distances between "H-20" and "H-22", "H-21a" and "H-24", and "H-21b" and "H-24" should be 0-3 Å (based on relevant coupling constants and ROESY correlations for Nemamide A; see Supplementary Table 1 and Supplementary Fig. 3). The CD spectra of the low energy conformers of the model compounds were then calculated using time dependent density functional theory (B3LYP functional/ 6-31G(d) basis set) with Gaussian 09. No UV shift correction was required. A sigma value of 0.16 eV was applied to the simulated CD spectra in SpecDis 1.60. The calculated CD spectra for the low energy conformers of each model compound were then Boltzmann-averaged.[3] The calculated CD spectra of the two model compounds are not exact mirror images because a defined (rather than infinite) number of low energy conformations were used to generate the Boltzmann-averaged CD spectrum.[5,6]

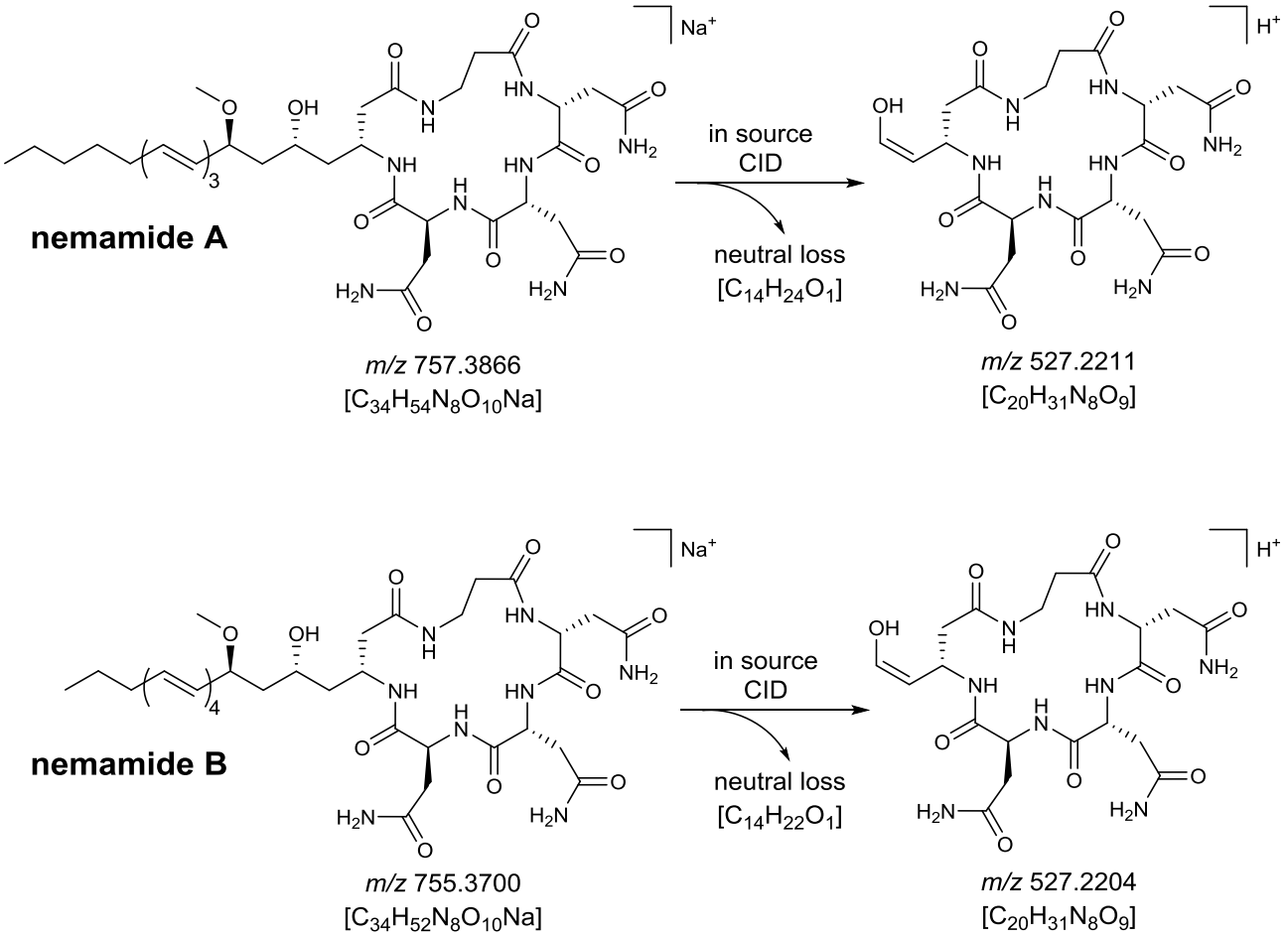

Supplementary Figure 10. In-source collision-induced dissociation (CID) of nemamide A and B. Both nemamide A and B undergo a neutral loss to yield the same product ion, indicating that the additional double bond in nemamide B is located in the neutral loss fragment.

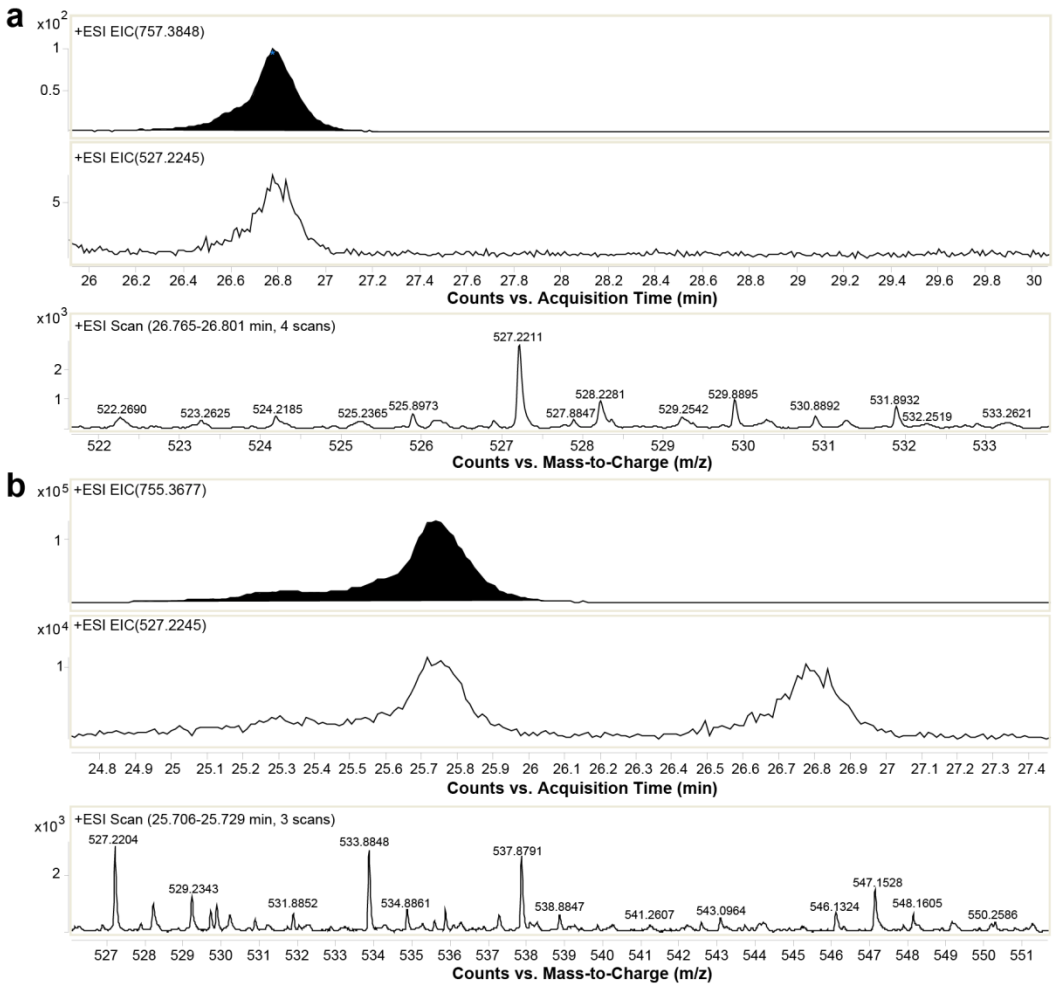

Supplementary Figure 11. High-resolution LC-MS data for in-source collision-induced dissociation (CID) of nemamide A and B. Raw data for nemamide A (**a**) and nemamide B (**b**) that serve as the basis for Supplementary Figure 10.

Supplementary Figure 12. NMR spectra for nemamide B in dimethyl sulfoxide-d_6.

(**a**) ^{1}H NMR spectrum (with water suppression, contaminant peaks are indicated with asterisks).

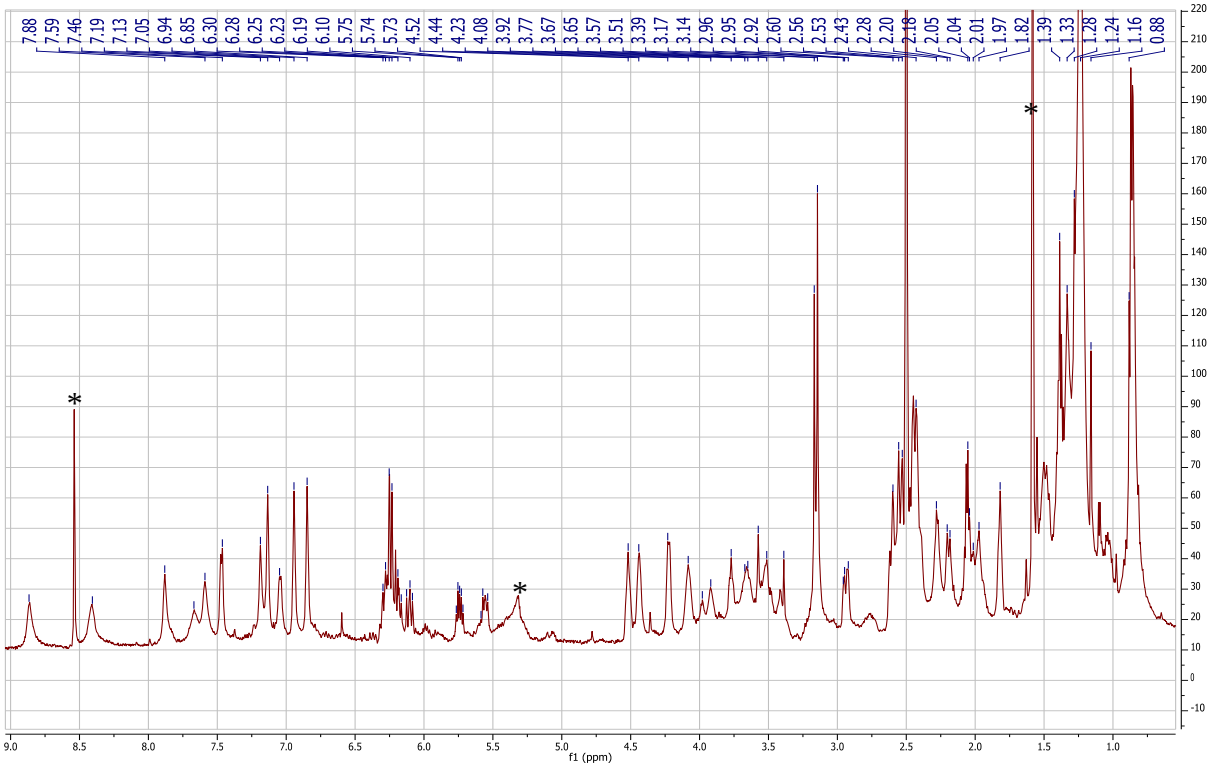

(**b**) ^{1}H NMR spectrum (without water suppression, contaminant peaks are indicated with asterisks).

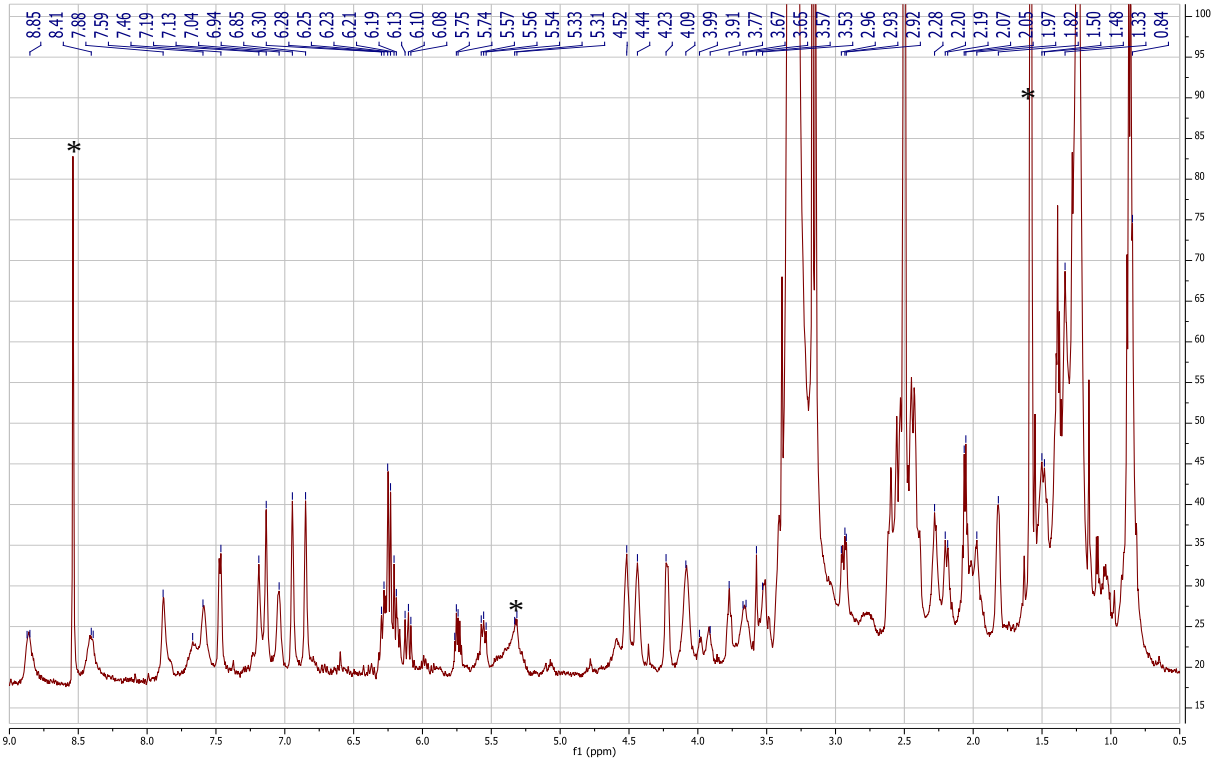

(**c**) dqf-COSY spectrum.

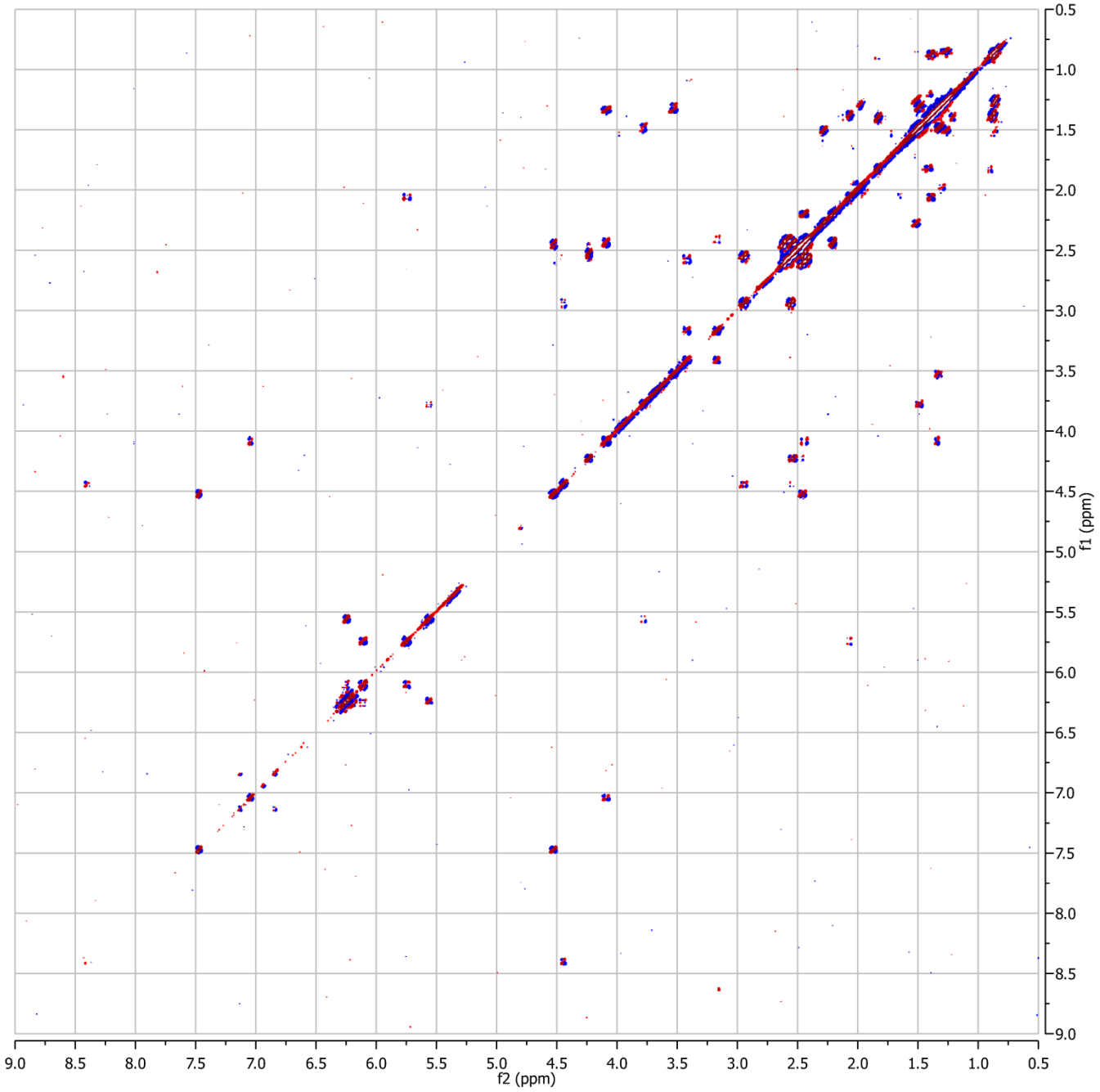

(**d**) dqf-COSY spectrum (0.5-5ppm region).

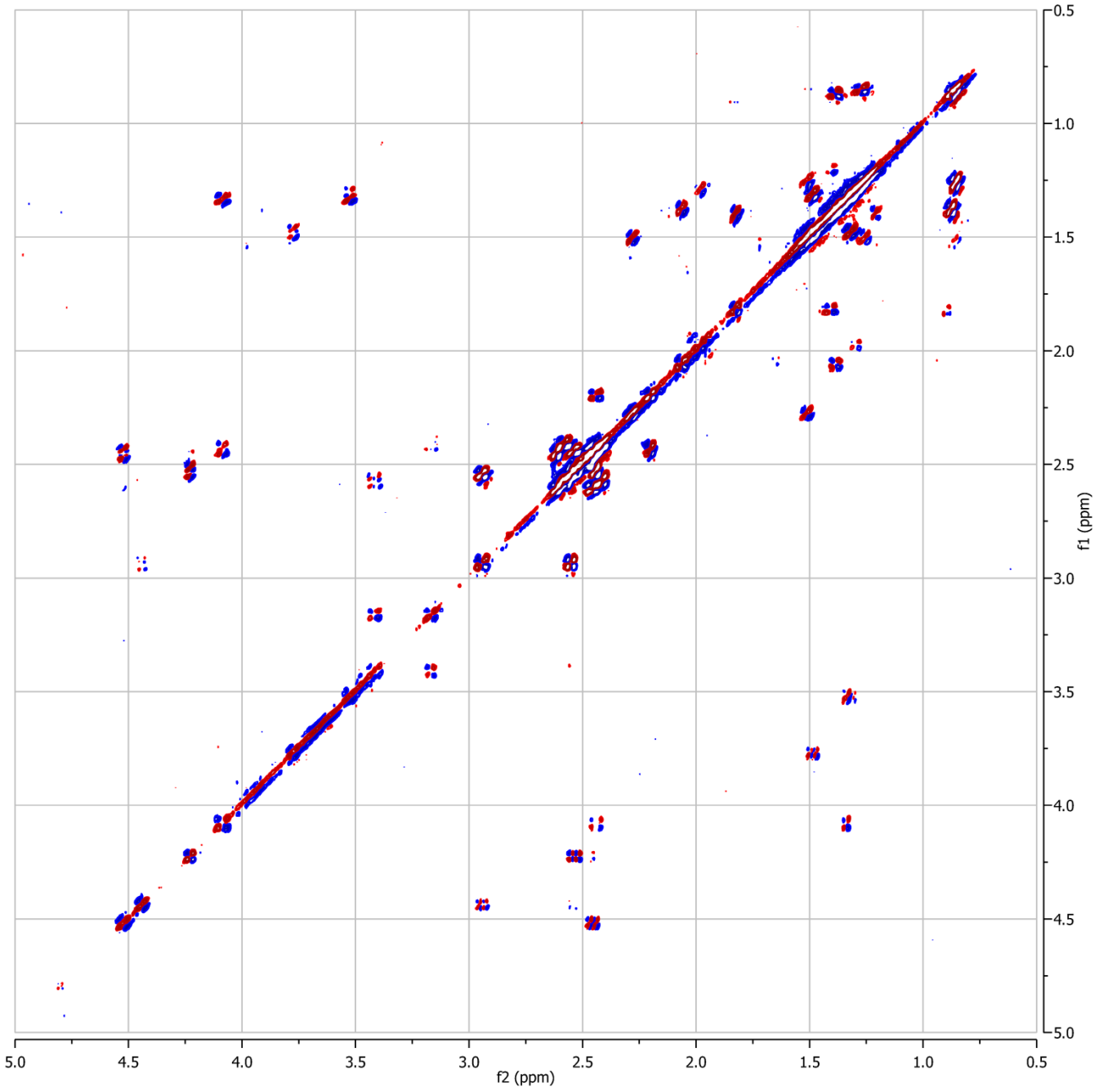

(**e**) TOCSY spectrum.

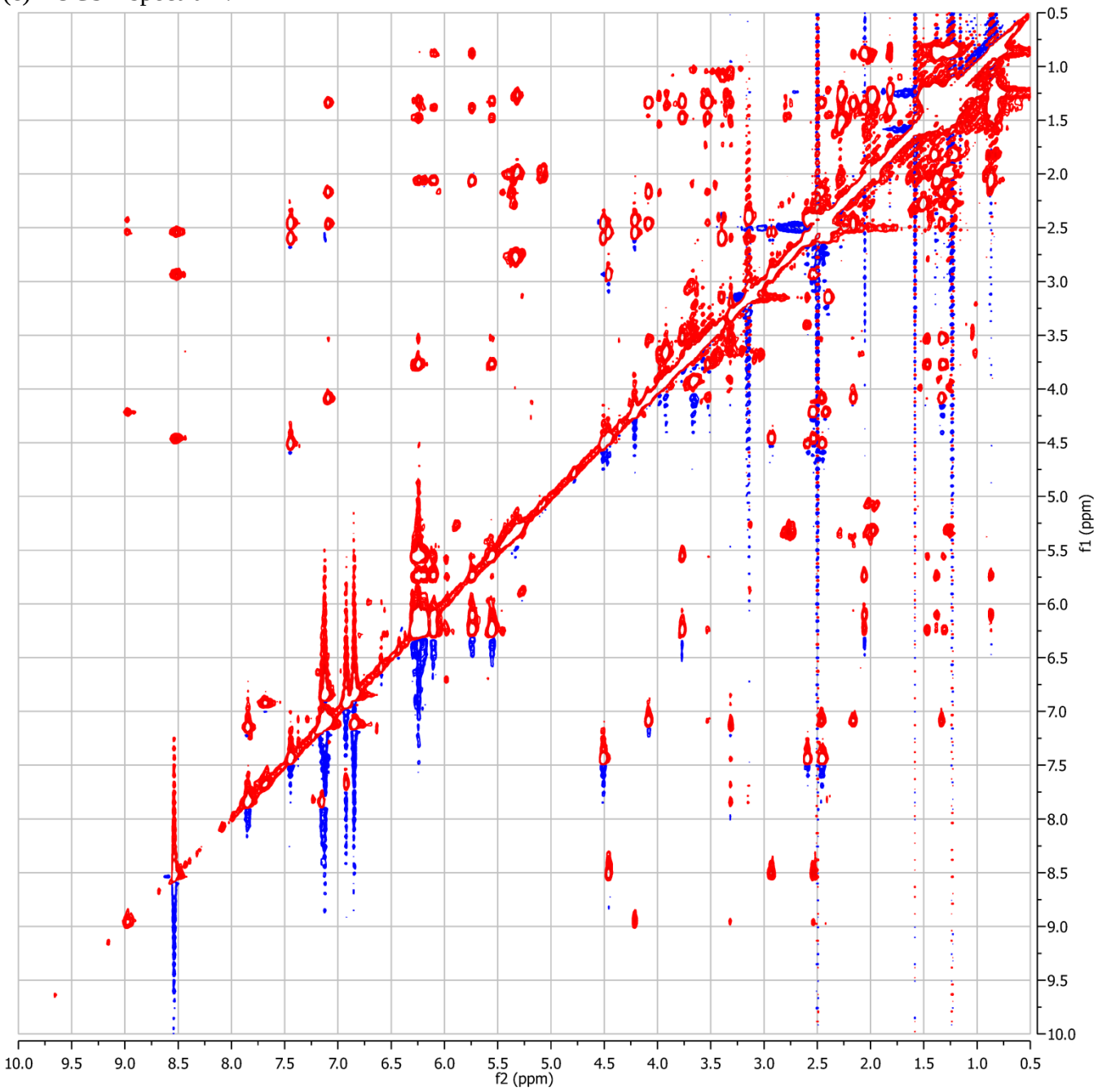

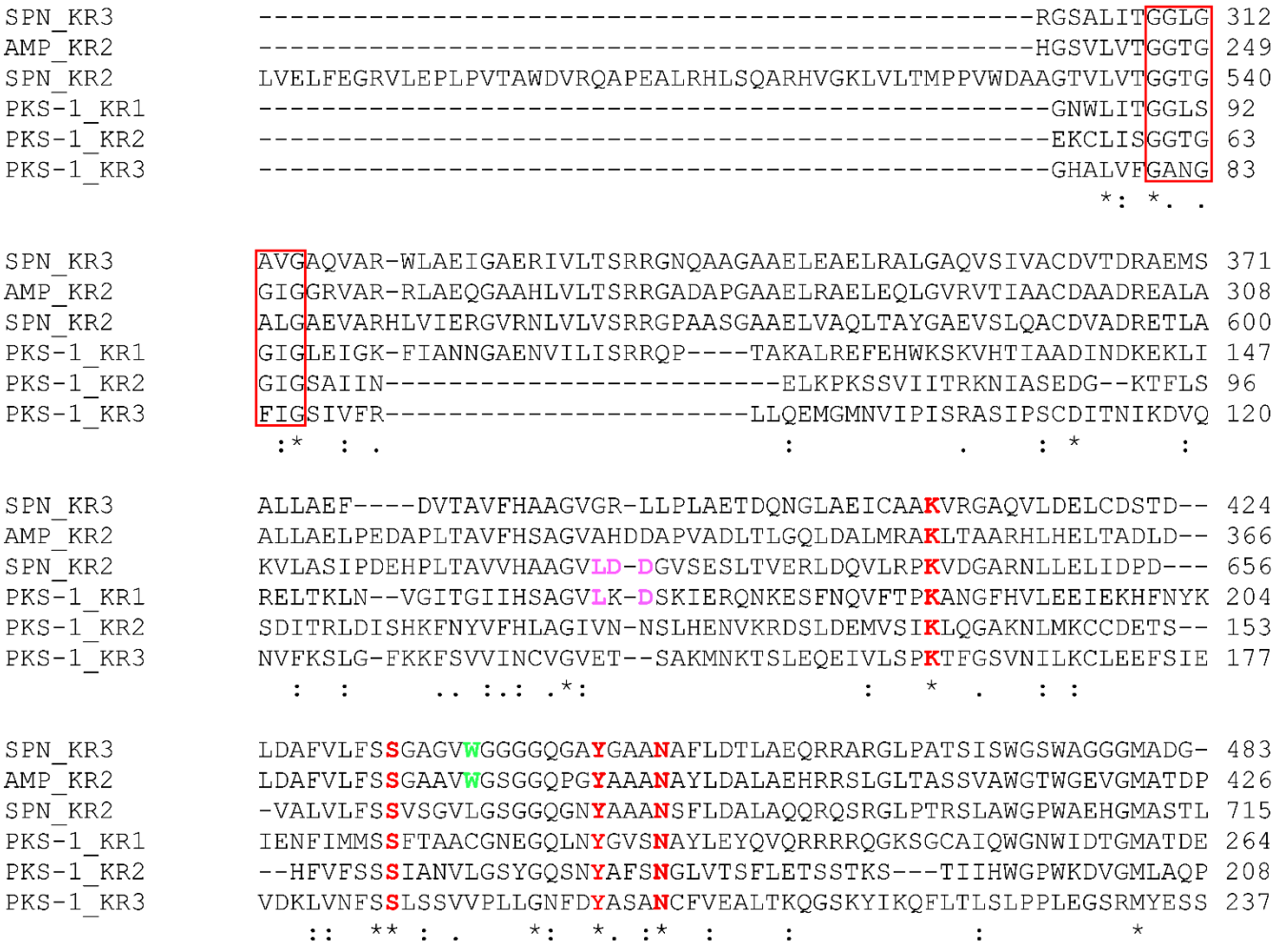

Supplementary Figure 13. Alignment of the PKS-1 KR domains with bacterial KR domains. The three ketoreductase (KR) domains in PKS-1 (KR_1, KR_2, and KR_3) were aligned with bacterial KR domains, SPN_KR3 and AMP_KR2 (A-type) and SPN_KR2 (B-type). Whereas A-type KR domains catalyze the formation of an L-configured alcohol at the 3-position relative to the thioester in the growing polyketide, B-type KR domains catalyze the formation of a D-configured alcohol at the 3 position relative to the thioester.[7] The PKS-1 KR_1 is a B-type KR domain, which provides further support for the assigned configuration at C-22 in nemamide A. Although PKS-1 KR_1 has an LKD motif instead of an LDD motif, the LKD sequence is seen in the chicken FAS KR domain, which is presumed to be a B-type KR domain.[8] PKS-1 KR_2 and KR_3 do not have characteristic residues of either an A-type or a B-type KR domain. Sequences were aligned with Clustal Omega.[9] KR domains are from spinosyn (Spn) and amphotericin (Amp) PKSs. Red boxes indicate possible NADP binding domains, red residues indicate catalytic residues, pink residues ("LDD") are characteristic of B-type KR domains, and green residues ("W") are characteristic of A-type KR domains.

```
PKS-1_TE     EIAAH---AGNKRIFVMGHSMGGIMSREIVAELK-IWGYDIPFVMLFDSWVLRTNELDIE    107
NRPS-1_TE    ESAEN---IETSKLVFIGASSAGTFAFSTSQLFA-DDD---VTVLLLDTG----------    274
SOR_P_TEI    TTLAC---ARNSPFVLFGHSSGGNIAHMVAEHLE-SIGHGPAGVVLLDSY----DYASPA    110
AMP_P_TEI    SVLMA---SDGEPFVMVGHSTGGSLAYLAAGVLEDTWGVKPEAVVLLDTASIRYNPSEGN    114
SPN_P_TEI    AVLQE---FAGGSFVLVGHSSGGWLAHEVAGELE-RRGVVPAGVVLLDTY----IPGEIT    109
SPI_P_TEI    AIVRS---TAGSPFAIVAYSSSGWLAYATASCLE-SKGSSPRALVLLDHV----DQ----    104
AVE_P_TEI    AIVRF---TDGAPFALAGHSAGGWFVYAVTSHLE-RLGVRPEAVVTMDAY----LPDDGI    110
PIK_P_TEI    AILRA---AGDAPVVLLGHSGGALLAHELAFRLERAHGAPPAGIVLVDPY----PPGHQE    115
ERY_P_TEI    AVIRT---QGDKPFVVAGHSAGALMAYALATELL-DRGHPPRGVVLIDVY----PPGHQD    109
BAC_N_TEI    IIKNI---QGEGPYTLIGYSSGGILAFDVAKELN-RQGYEVEDLIIIDSK----YRTKAE    97
TYR_N_TEI    AITAI---DPSGPYTLMGYSSGGNLAFEVAKELE-ERGYGVTDIILFDSY----WKDKAI    97
SUR_N_TEI    LIQKL---QPEGPLTLFGYSAGCSLAFEAAKKLE-GQGRIVQRIIMVDSY----KKQGVS    114
MYX_PN_TEI   EVRKV---RPKGPYRLGGWSTGGILAQAMARQLE-EAGEQVELLMLLETW----SPTVYQ    104
HEC_PN_TEI   AIKSV---QPKGPYLLGGHSFGGLVAFETAQQLQ-KQGDEVAKLFIIDMR----APAVDK    108
TUB_PN_TEI   ELREL---QPRGPYRLGGWSFGCVVAYEVALQLE-AAGEQVALLSLLDFP----APSGQR    108
CHO_PN_TEI   AIQQI---QPSGPYHLGGHSAGARIAFAVALELQ-RRGAEVPLVSIVDMR----PPGRGA    105
MEG_P_TEII   VLRDL---VGEVPFALFGHSMGALVAYETARRLEARPGVRPLRLFVSGQT----APRVHE    126
PIK_P_TEII   ATEPW---WQEGRLAFFGHSLGASVAFETARILEQRHGVRPEGLYVSGRR----APSLAP    135
BOR_P_TEII   VLRA----RVHQPVALFGHSMGATLAFELARRFESAGIS-LEALLVSARP----APSRQR    131
TYL_P_TEII   ELRRLLDAPDGVPVALFGHSMGAVVAYETARLLHRSGAPRPAGLILSGRR----APTADR    151
KEN_P_TEII   ALGA---RSDGRPFALFGHSMGSLVAFETARRLQTRGA-APSVLFASGRP----APSCLR    128
RIF_P_TEII   VLRP----FGDRPLALFGHSMGAIIGYELALRMPEAGLPAPVHLFASGRR----APSRYR    130
BAC_N_TEII   QVQAE---RKGDDYALFGHSMGSLLAYELYYQMSGAGAEKPVHIFFSGYK----APNRIR    111
MIC_N_TEII   AILP----HLTKPFAFFGHSMGGLVSFELARLLRKEYNQSPLHLFVSGYR----APQIPD    138
```

Supplementary Figure 14. Alignment of PKS-1 and NRPS-1 TE domains with bacterial TE domains. The PKS-1 and NRPS-1 TE domains were aligned with bacterial TEI and TEII domains. TEI domains cleave polyketides/nonribosomal peptides from PKS/NRPSs once biosynthesis is complete, while TEII domains have editing functions.[10] Both the PKS-1 TE domain and the NRPS-1 TE domain have the Ser-Asp-His catalytic triad of TEI domains. Red residues indicate catalytic residues (portion of sequence alignment showing conserved His is not shown). Although the PKS-1 TE domain appears to be most similar to PKS-NRPS TEI domains (see Supplementary Fig. 15), it does have the sequence motif around the catalytic Ser (GHSMG) that is characteristic of TEII domains. Sequences were aligned with Clustal Omega.[9] TE domains are from the PKS (P), NRPS (N), and PKS-NRPS (PN) assembly lines that biosynthesize soraphen (Sor), amphotericin (Amp), spinosyn (Spn), spirangien (Spi), avermectin (Ave), pikromycin (Pik), erythromycin (Ery), bacitracin (Bac), tyrocidine (Tyr), surfactin (Sur), myxothiazol (Myx), hectochlorin (Hec), tubulysin (Tub), chondramid (Cho), megalomicin (Meg), borrelidin (Bor), tylosin (Tyl), kendomycin (Ken), rifampicin (Rif), and microcystein (Mic).

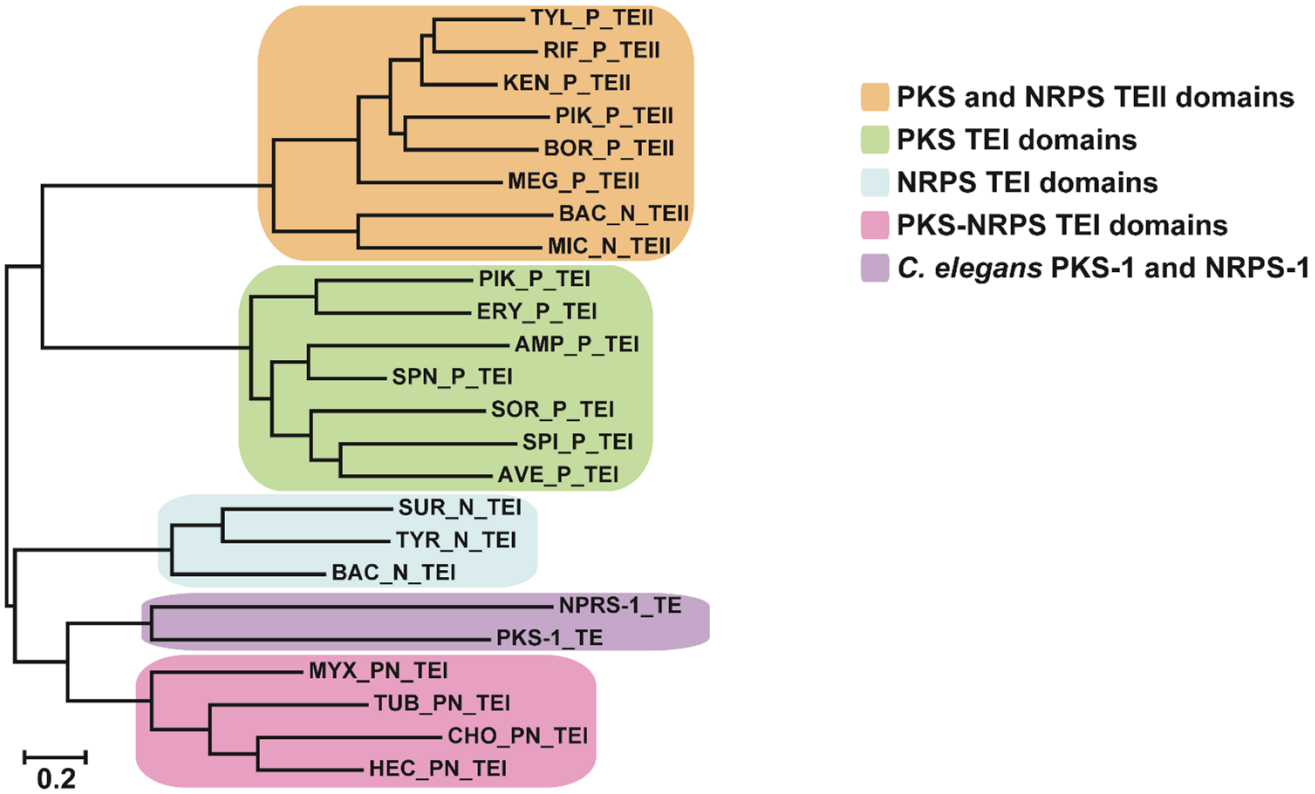

Supplementary Figure 15. Phylogeny of the PKS-1 and NRPS-1 TE domains and bacterial TE domains. Both the PKS-1 and NRPS-1 TE domains cluster with the TEI domains of bacterial hybrid PKS-NRPSs. TE domains are described in Supplementary Figure 14. Phylogenetic tree was generated in MEGA 6.[11]

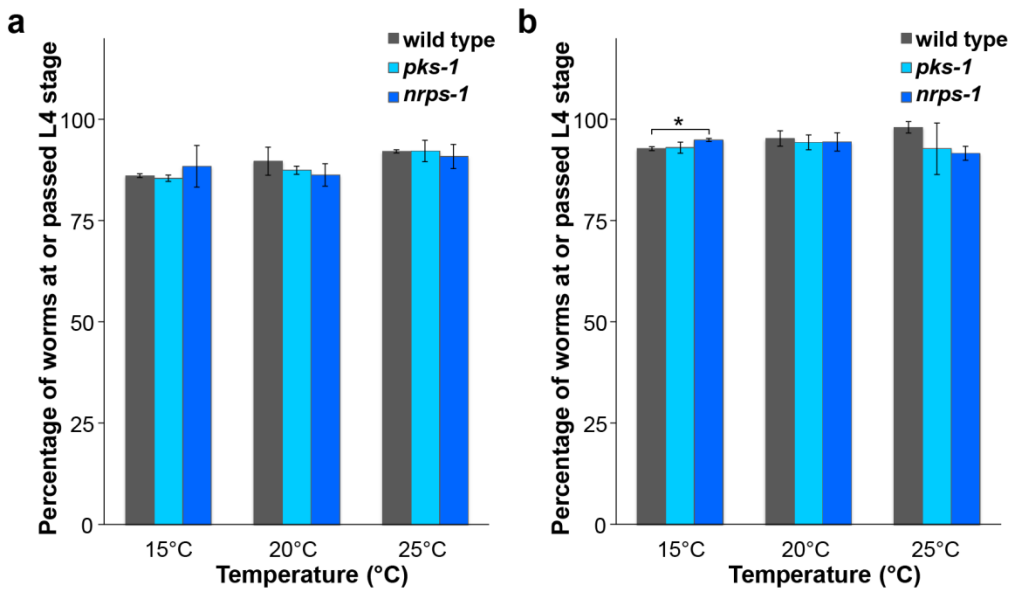

Supplementary Figure 16. Comparison of development of wild-type, *pks-1*, and *nrps-1* worms. (**a**) Development of eggs (obtained through alkaline-bleach treatment of gravid adults) to the L4 stage for wild-type, *pks-1*, and *nrps-1* worms at different temperatures. Eggs were obtained using a similar method as in Figure 2c, but were hatched in food such that they did not go through L1 arrest. The lack of difference between wild type and mutants suggests that the delayed L1 recovery of the mutants seen in **Figure 2c** is not due to the alkaline-bleach treatment or to a general delay in developmental rate. (**b**) Development of eggs (obtained by allowing gravid adults to lay eggs) to the L4 stage for wild-type, *pks-1*, and *nrps-1* worms at different temperatures. The lack of difference between wild type and mutants suggests that the delayed L1 recovery of the mutants seen in **Figure 2c** is not due to a general delay in developmental rate. Data represent the mean ± SD of two independent experiments. Two-tailed, unpaired t-tests were used to determine statistical significance. All *P* values were non-significant except as indicated (*$P \leq 0.05$).

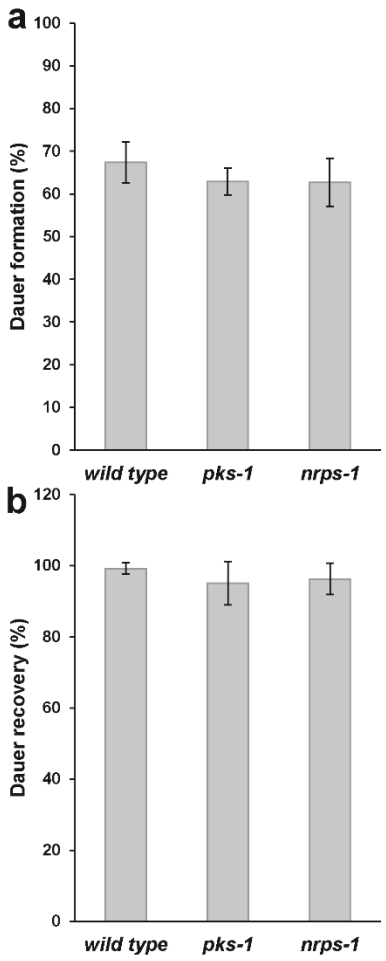

Supplementary Figure 17. Dauer formation and recovery in wild-type, *pks-1*, and *nrps-1* worms. (**a**) Dauer formation in wild-type, *pks-1*, and *nrps-1* worms exposed to 1 μM asc-C6-MK (ascr#2) in the dauer formation assay at 25 °C. (**b**) Recovery of wild-type, *pks-1*, and *nrps-1* dauers after being placed on a lawn of OP50 bacteria for 24h at 20 °C. Data represent the mean ± SD of two (**a**) or four (**b**) independent experiments. In (**a**) and (**b**), two-tailed, unpaired t-tests showed that there is no significant difference between the wild type and mutants.

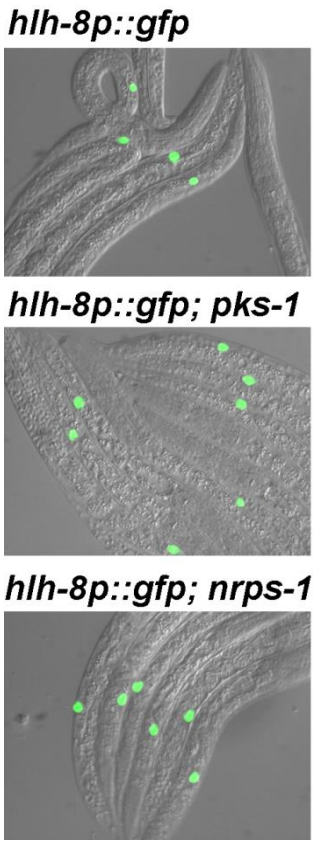

Supplementary Figure 18. M-cell imaging in wild-type, *pks-1* and *nrps-1* backgrounds. Fluorescence images showing that the M-cell (identified using the M-cell-specific reporter, *hlh-8p:gfp*) does not divide during L1 arrest in wild-type, *pks-1*, and *nrps-1* worms. M-cell arrest in arrested L1s is an indication that the worm has properly arrested somatic progenitor cell division during starvation. Certain mutants in the insulin/IGF-1 pathway, such as *daf-16/foxo*, undergo improper M-cell division during L1 arrest.[12,13]

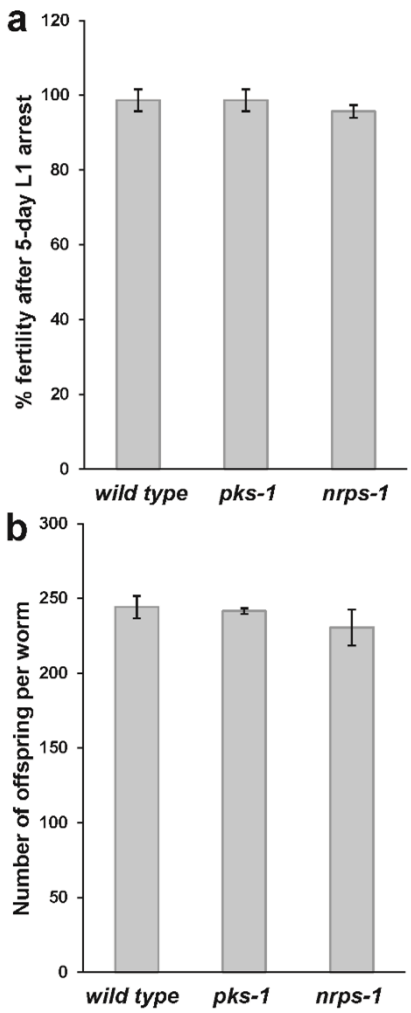

Supplementary Figure 19. Fertility and brood size in wild-type, *pks-1* and *nrps-1* worms that experienced extended L1 arrest. Percent fertility (**a**) and brood size (**b**) after L1s were subjected to five days of L1 arrest and then allowed to recover and develop into adults on food. The absence of fertility defects in the mutants suggests that the mutants maintain proper germline arrest during starvation-induced L1 arrest. Certain mutants in the insulin/IGF-1 pathway, such as *daf-18/pten*, undergo improper germline proliferation during L1 arrest, leading to fertility defects once the L1 recover and develop to the adult stage.[14,15] Data represent the mean ± SD of five independent experiments (n = 30) (**a**) or two independent experiments (n = 20) (**b**). In (**a**) and (**b**), two-tailed, unpaired t-tests showed that there is no significant difference between the wild type and the mutants.

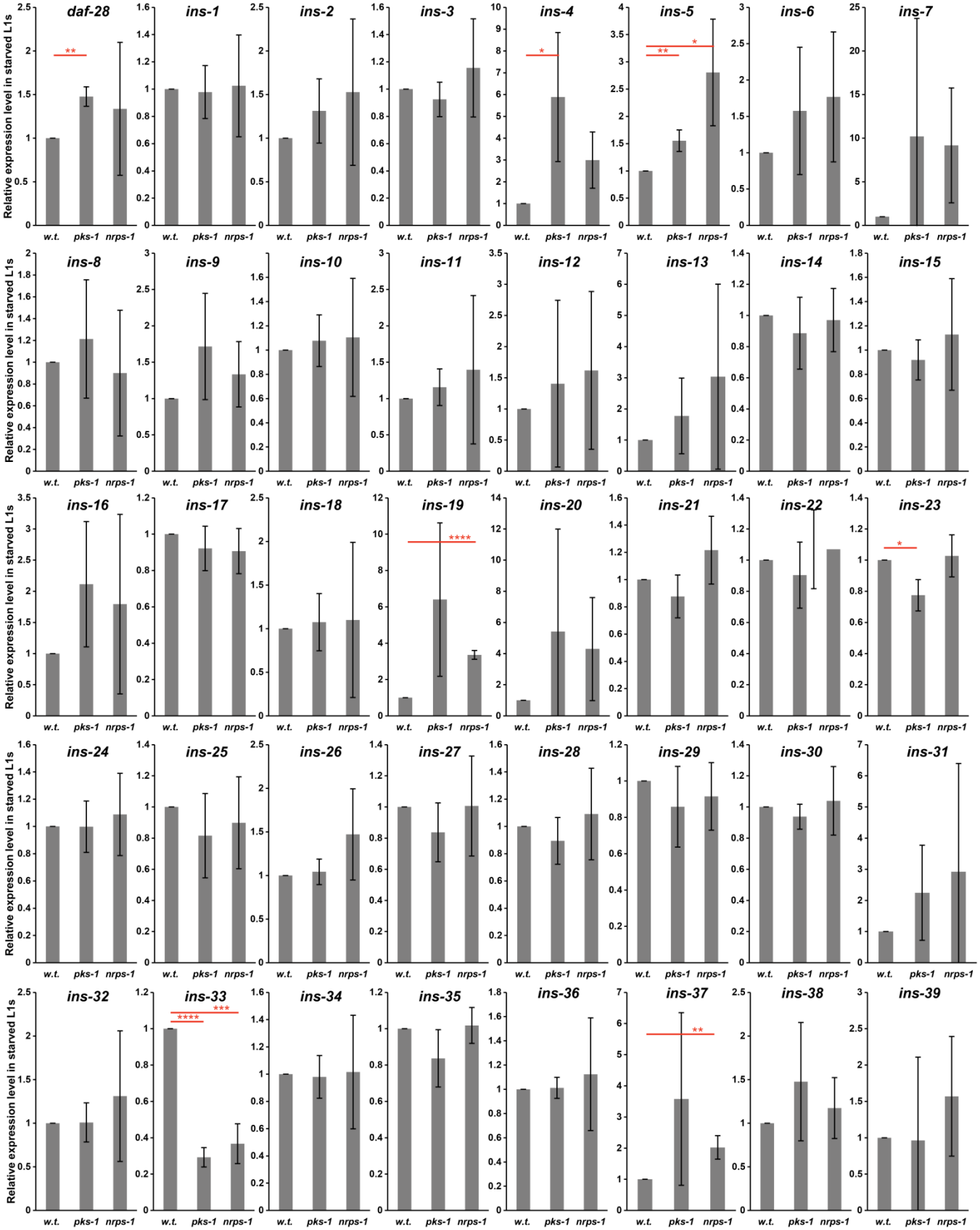
daf-28
ins-1
ins-2
ins-3
ins-4
ins-5
ins-6
ins-7
ins-8
ins-9
ins-10
ins-11
ins-12
ins-13
ins-14
ins-15
ins-16
ins-17
ins-18
ins-19
ins-20
ins-21
ins-22
ins-23
ins-24
ins-25
ins-26
ins-27
ins-28
ins-29
ins-30
ins-31
ins-32
ins-33
ins-34
ins-35
ins-36
ins-37
ins-38
ins-39
Relative expression level in starved L1s
w.t.
pks-1
nrps-1

Supplementary Figure 20. Expression of insulins in wild-type, *pks-1*, and *nrps-1* arrested L1s relative to wild-type arrested L1s, as determined by qRT-PCR. *ins-4*, *ins-5*, *ins-19*, and *ins-37* are expressed at higher levels in *pks-1* and/or *nrps-1* arrested L1s than in wild-type arrested L1s. *daf-28* is also expressed at higher levels in *pks-1* arrested L1s than in wild-type arrested L1s. Conversely, *ins-33* is expressed at lower levels in *pks-1* and *nrps-1* arrested L1s than in wild-type arrested L1s. Higher levels of expression of *ins-4* and *daf-28* in arrested L1s have been associated with reduced L1 arrest survival, and deletion of *ins-4* and *daf-28* has been associated with increased L1 arrest survival.[16] Data represent the mean ± SD of three independent experiments. Two-tailed, unpaired t-tests were used to determine statistical significance (*$P \leq 0.05$, **$P \leq 0.01$, ***$P \leq 0.001$, ****$P \leq 0.0001$).

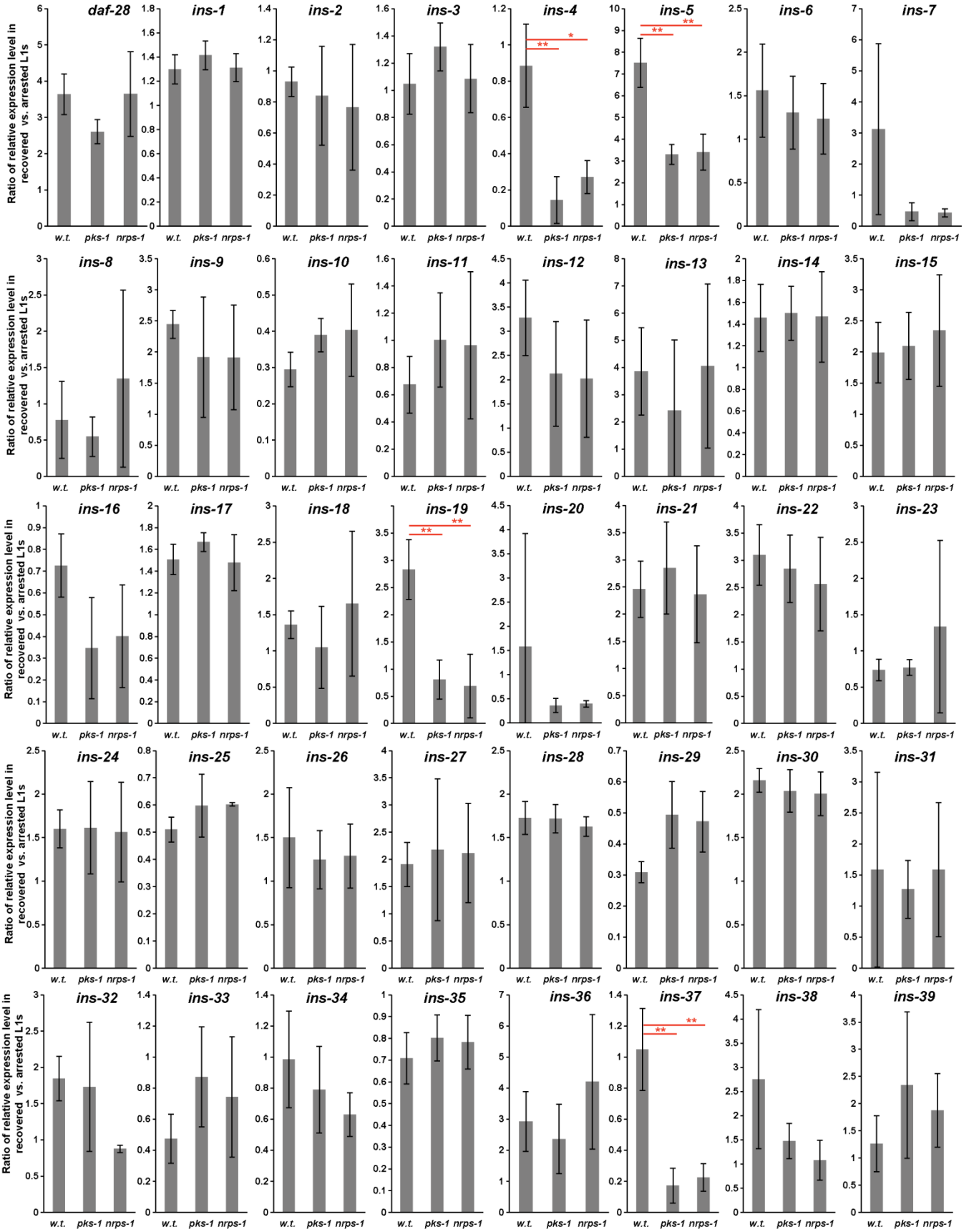
daf-28
ins-1
ins-2
ins-3
ins-4
ins-5
ins-6
ins-7
ins-8
ins-9
ins-10
ins-11
ins-12
ins-13
ins-14
ins-15
ins-16
ins-17
ins-18
ins-19
ins-20
ins-21
ins-22
ins-23
ins-24
ins-25
ins-26
ins-27
ins-28
ins-29
ins-30
ins-31
ins-32
ins-33
ins-34
ins-35
ins-36
ins-37
ins-38
ins-39
Ratio of relative expression level in recovered vs. arrested L1s
w.t.
pks-1
nrps-1
pks-1 nrps-1
*
**

Supplementary Figure 21. Expression of insulins in recovered versus arrested wild-type, *pks-1*, and *nrps-1* L1s, as determined by qRT-PCR. *ins-5* and *ins-19* are induced during recovery in wild-type L1s, but not induced (or not induced as much) in *pks-1* and *nrps-1* L1s. *ins-4* and *ins-37* are not induced during recovery (at least not at 6h post-recovery) in wild-type L1s, but are down-regulated in *pks-1* and *nrps-1* L1s. Data represent the mean ± SD of three independent experiments. Two-tailed, unpaired t-tests were used to determine statistical significance (*$P \leq 0.05$, **$P \leq 0.01$, ***$P \leq 0.001$, ****$P \leq 0.0001$).

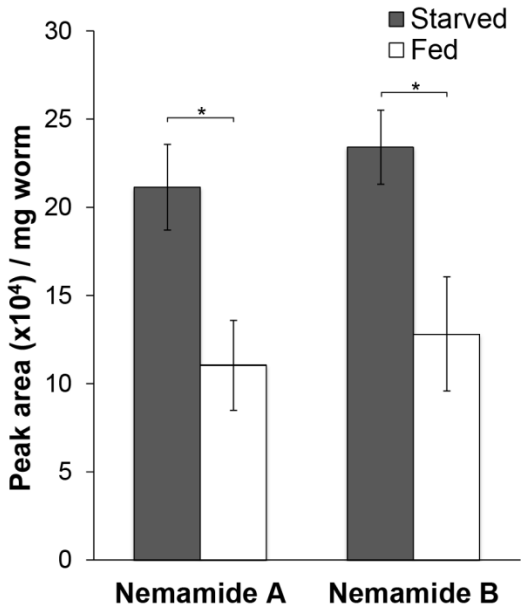

Supplementary Figure 22. Nemamide production in arrested and recovered L1s. Levels of nemamides A and B in arrested L1s and recovered L1s (6 h after addition of food). Data represent the mean ± SD of four independent experiments. Two-tailed, unpaired t-tests were used to determine statistical significance (*$P \leq 0.05$).

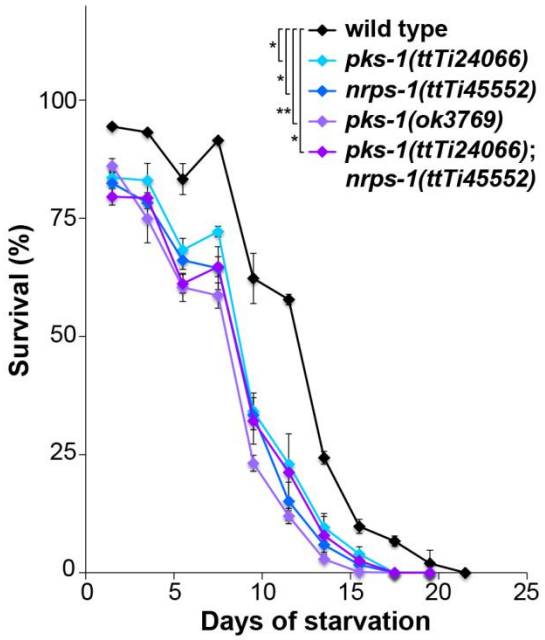

Supplementary Figure 23. L1 survival for wild-type and different mutant strains. In addition to the *pks-1(ttTi24066)* and *nrps-1(ttTi45552)* strains (which were the *pks-1* and *nrps-1* alleles used throughout this manuscript), we also tested L1 survival in the *pks-1(ok3769)* strain and the *pks-1(ttTi24066)*; *nrps-1(ttTi45552)* double mutant strain and obtained similar results. That is, no statistically significant difference was found for any of the tested mutants in terms of mean survival. The mean ± SD of three independent experiments are plotted. Mean survival (days ± SE) was calculated as described in Methods: 12.2±0.3 for wild type, 9.4±0.4 for *pks-1(ttTi24066)*, 8.9±0.4 for *nrps-1(ttTi45552)*, 7.7±0.4 for *pks-1(ok3769)*, and 8.7±0.5 for *pks-1(ttTi24066)*; *nrps-1(ttTi45552)*. A two-tailed, unpaired t-test was used to determine statistical significance (*$P \leq 0.05$, **$P \leq 0.01$, ***$P \leq 0.001$).

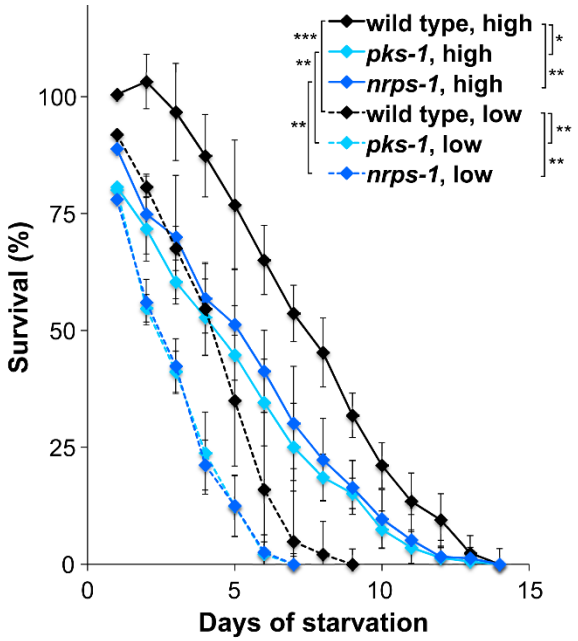

Supplementary Figure 24. L1 survival for wild-type, *pks-1*, and *nrps-1* worms at low and high population densities. Survival assays were performed at 25 °C. The mean ± SD of three independent experiments are plotted. Mean survival (days ± SE) was calculated as described in Methods: 8.3±0.2 for wild type/high, 6.4±0.4 for *pks-1*/high, 5.9±0.4 for *nrps-1*/high, 5.2±0.3 for wild type/low, 2.8±0.4 for *pks-1*/low, and 2.9±0.4 for *nrps-1*/low. A two-tailed, unpaired t-test was used to determine statistical significance (*$P \leq 0.05$, **$P \leq 0.01$, ***$P \leq 0.001$).

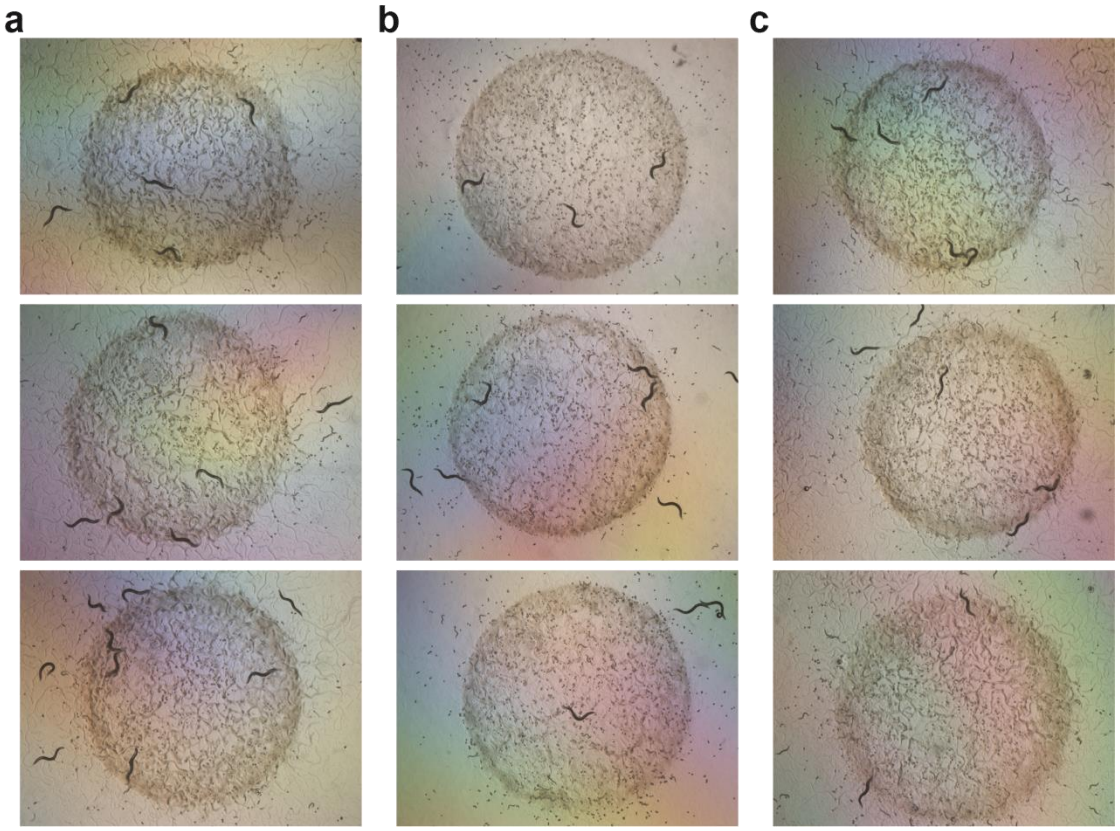

Supplementary Figure 25. Feeding rate of wild-type, *pks-1*, and *nrps-1* worms. Ten wild-type, *pks-1*, or *nrps-1* worms at the L4 stage were transferred to NGM-agar plates (containing 50 μM of 5-fluoro-2'-dexoxyuridine to prevent egg development) with a lawn of OP50 bacteria. The plates were incubated at 20 °C. The rate that the bacterial lawn was consumed was monitored over time, and no differences between the worms strains were observed. Photos of the plates with the wild-type (**a**), *pks-1* (**b**), and *nrps-1* (**c**) worms were taken after 6 d. Three replicates were done for each strain.

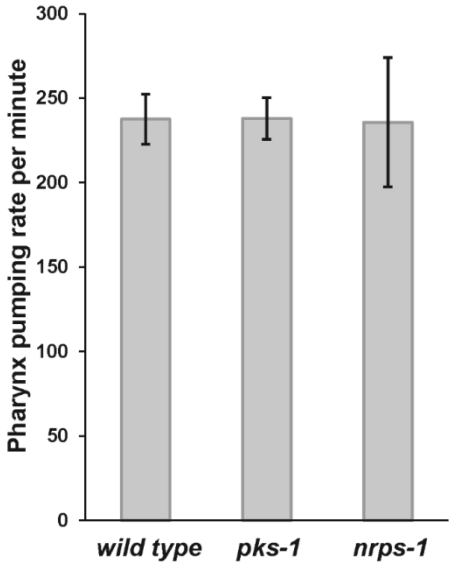

Supplementary Figure 26. Pharynx pumping rate of wild-type, *pks-1*, and *nrps-1* worms. Data represent the mean ± SD of two independent experiments. Two-tailed, unpaired t-tests showed that there is no significant difference between the wild type and the mutants.

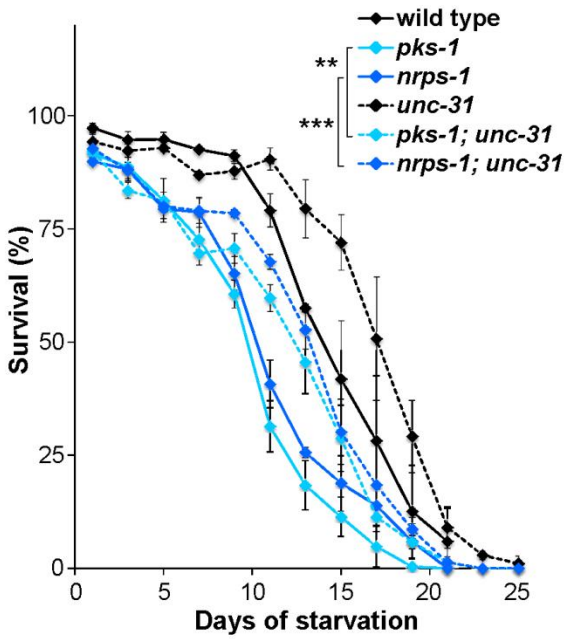

Supplementary Figure 27. Effect of an *unc-31(e928 null)* mutation on survival of arrested L1s. UNC-31 regulates insulin secretion and acts upstream of the insulin/IGF-1 pathway, which controls L1 survival in a manner dependent on the *daf-16/foxo* transcription factor.[12,17,18] The *unc-31(e928 null)* mutation was able to suppress significantly, but not completely, the reduced survival of the *pks-1* and *nrps-1* mutants. Thus, the nemamides likely extend L1 survival by negatively regulating UNC-31-mediated insulin signaling and UNC-31-independent pathways. Survival assays were performed at 20°C. Mean survival (days ± SE) was calculated as described in Methods: 14.3 ± 0.2 for wild type, 10.0 ± 0.2 for *pks-1*, 10.9 ± 0.2 for *nrps-1*, 17.5 ± 0.2 for *unc-31*, 13.1 ± 0.3 for *pks-1; unc-31*, and 13.9 ± 0.2 for *nrps-1; unc-31*. Data represent the mean ± SD of three independent experiments. A two-tailed, unpaired t-test was used to determine statistical significance (*$P \leq 0.05$, **$P \leq 0.01$, ***$P \leq 0.001$).

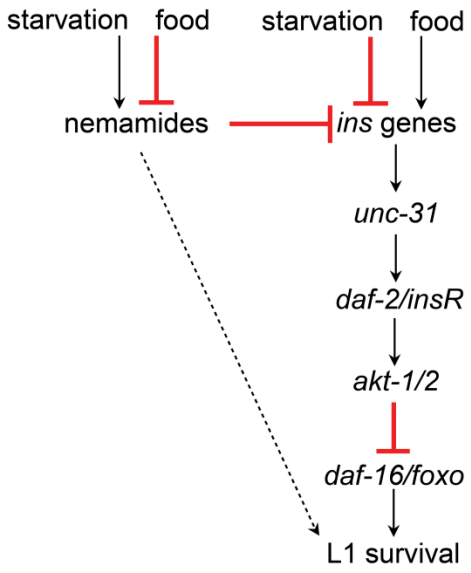

Supplementary Figure 28. Model for the role of the nemamides in L1 arrest and survival.

Supplementary Table 1. ^{1}H and ^{13}C NMR data derived from ^{1}H, dqf-COSY, HSQC, and HMBC spectra for nemamide A in dimethyl sulfoxide-d_6.

#	δ_H (J (Hz))	δ_C	HMBC
1		171.1	
2	4.51, m ($J_{2,3a}$ = 9.0; $J_{2,3b}$ = 6.9)	50.1	C_1
2-NH	7.46, brd ($J_{2,2\text{-NH}}$ = 8.1)		C_5
3a	2.45, overlap ($J_{3a,3b}$ = 15.9)	36.9	C_1, C_2
3b	2.61, overlap	36.9	C_1
4		171.3	
4-NH_2a	6.85, brs ($J_{4\text{-NH2a},4\text{-NH2b}}$ = 4.8)		C_3
4-NH_2b	7.14, brs		C_4
5		170.7	
6	4.45, m ($J_{6,7a}$ = 4.9; $J_{6,7b}$ = 6.6)	49.3	
6-NH	8.42, brs ($J_{6,6\text{-NH}}$ = 8.2)		
7a	2.56, overlap ($J_{7a,7b}$ = 16.6)	35.8	C_5, C_8
7b	2.95, dd	35.8	C_6, C_8
8		173.3	
8-NH_2a	7.18, brs ($J_{8\text{-NH2a},8\text{-NH2b}}$ = 4.9)		C_7
8-NH_2b	7.86, brs		
9		170.9	
10	4.22, m ($J_{10,11a}$ = 6.7; $J_{10,11b}$ = 9.6)	52.5	
10-NH	8.86, brs ($J_{10,10\text{-NH}}$ = 3.4)		
11a	2.44, overlap ($J_{11a,11b}$ = 17.8)	35.9	C_9, C_{12}
11b	2.53, overlap	35.9	C_9, C_{10}
12		173.1	
12-NH_2a	6.95, brs ($J_{12\text{-NH2a},12\text{-NH2b}}$ = 4.8)		C_{11}
12-NH_2b	7.58, brs		
13		173.4	
14a	2.41, overlap ($J_{14a,15a}$ = 8.9)	33.3	C_{13}
14b	2.57, overlap ($J_{14a,14b}$ = 18.5)	33.3	C_{13}
15a	3.15, overlap ($J_{15a,15b}$ = 15.9)	34.8	
15b	3.42, overlap ($J_{14b,15b}$ = 9.6)	34.8	
15-NH	7.73, brs		
16		170.3	
17a	2.18, brd ($J_{17a,17b}$ = 14.5)	40.6	C_{16}
17b	2.47, overlap ($J_{17b,18}$ = 9.8)	40.6	C_{16}
18	4.08, m ($J_{18,19}$ =6.7)	44.9	
18-NH	7.05, brs ($J_{18,18\text{-NH}}$ = 8.2)		C_1
19	1.32, m ($J_{19,20}$ = 6.7)	43.7	C_{17}, C_{18}, C_{20}, C_{21}
20	3.51, m ($J_{20,21a}$ = 8.2)	63.3	
20-OH	4.55, brs		
21a	1.30, m ($J_{21a,21b}$ =14.5)	43.5	
21b	1.48, m ($J_{21b,22}$ = 9.8)	43.5	C_{22}
22	3.76, m ($J_{22,24}$ = 7.5)	77.6	C_{23}, C_{25}
23	3.13, s	55.5	C_{22}
24	5.51, dd ($J_{24,25}$ = 15.4)	133.7	C_{22}, C_{26}
25	6.19, dd ($J_{25,26}$ = 11.2)	131.3	C_{22}, C_{24}
26	6.14, dd ($J_{26,27}$ = 14.5)	129.7	C_{24}, C_{28}
27	6.23, dd ($J_{27,28}$ = 10.7)	132.9	C_{25}, C_{26}, C_{29}
28	6.07, dd ($J_{28,29}$ = 15.1)	130.1	C_{26}, C_{30}
29	5.72, dt ($J_{29,30}$ = 7.0)	135.2	C_{27}, C_{30}, C_{31}
30	2.06, m	32.0	C_{28}, C_{29}, C_{31}, C_{32}
31	1.35, overlap	28.2	C_{29}, C_{30}, C_{32}, C_{33}
32	1.24, overlap	30.8	C_{30}, C_{31}, C_{33}, C_{34}
33	1.26, overlap ($J_{33,34}$ = 7.1)	21.8	C_{31}, C_{32}, C_{34}
34	0.86, t	13.8	C_{32}, C_{33}

Supplementary Table 2. ^{1}H and ^{13}C NMR chemical shifts derived from ^{1}H, TOCSY, HSQC, and HMBC spectra for the three cyclic peptides in dimethyl sulfoxide-d_6.

#	Cyclic Peptide **3** (2*S*,6*R*,10*R*,18*R*)		Cyclic Peptide **4** (2*R*,6*S*,10*R*,18*S*)		Cyclic Peptide **5** (2*R*,6*R*,10*S*,18*S*)	
	δ_H (J (Hz))	δ_C	δ_H (J (Hz))	δ_C	δ_H (J (Hz))	δ_C
1		169.7		169.6		170.1
2	4.48, m	49.9	4.49, m	49.7	4.40, m	50.9
2-NH	7.49, brd, ($J_{2,2\text{-NH}}$ = 8.1)		7.85, brd, ($J_{2,2\text{-NH}}$ = 8.8)		7.49, brd, ($J_{2,2\text{-NH}}$ = 7.9)	
3a	2.43, dd, ($J_{3a,3b}$ = 19.4; $J_{2,3a}$ =12.7)	36.8	2.43, dd, ($J_{3a,3b}$ = 15.8; $J_{2,3a}$ =6.9)	35.1	2.56, overlap	36.5
3b	2.62, dd, ($J_{3a,3b}$ = 19.3; $J_{2,3b}$ =6.5)	36.8	2.69, ($J_{3a,3b}$ = 15.8; $J_{2,3b}$ =5.6)	35.1	2.56, overlap	36.5
4		171.2		171.8		171.2
4-NH_2a	6.82, brs		6.85, brs		6.88, brs	
4-NH_2b	7.11, brs		7.38, brs		7.27, brs	
5		170.5		170.3		170.7
6	4.41, m	49.2	4.40, m	48.7	4.33, m	50.9
6-NH	8.20, brd, ($J_{6,6\text{-NH}}$ = 8.8)		7.81, brd, ($J_{6,6\text{-NH}}$ = 8.8)		8.89, brd, ($J_{6,6\text{-NH}}$ = 5.2)	
7a	2.58, brd, ($J_{7a,7b}$ = 17.2)	35.4	2.54, overlap	35.3	2.48, overlap	35.4
7b	2.98, dd, ($J_{7a,7b}$ = 16.4; $J_{6,7b}$ =4.7)	35.4	3.05, dd, ($J_{7a,7b}$ = 17.2; $J_{6,7b}$ =3.8)	35.3	2.60, overlap	35.4
8		173.6		173.8		170.9
8-NH_2a	7.32, brs		7.47, brs		6.89, brs	
8-NH_2b	7.80, brs		7.92, brs		7.33, brs	
9		171.1		170.2		173.9
10	4.25, m	52.1	4.46, m	49.3	4.40, m	50.9
10-NH	8.63, brs		8.39, brd, ($J_{10,10\text{-NH}}$ = 7.4)		8.48, brs	
11a	2.51, overlap	35.6	2.48, overlap	35.4	2.31, brd, ($J_{11a,11b}$ = 16.1)	35.6
11b	2.51, overlap	35.6	2.65 , ($J_{11a,11b}$ = 15.7; $J_{10,11b}$ =6.8)	35.4	2.49, overlap	35.6
12		173.6		172.3		170.3
12-NH_2a	6.96, brs		6.95, brs		6.98, brs	
12-NH_2b	7.43, brs		7.33, brs		7.40, brs	
13		173.3		172.6		172.3
14a	2.42, overlap	33.5	2.36, m	34.7	2.23, m	34.0
14b	2.57, overlap	33.5	2.48, overlap	34.7	2.56, overlap	34.0
15a	3.18, m	34.8	3.14, overlap	34.3	3.33, overlap	35.4
15b	3.42, m	34.8	3.55, overlap	34.3	3.33, overlap	35.4
15-NH	7.36, brs		7.25, brs		7.00, brs	
16		170.7		170.2		170.0
17a	2.15, brd, ($J_{17a,17b}$ = 12.0)	41.4	2.11, brd, ($J_{17a,17b}$ = 11.3)	41.5	2.06, dd, ($J_{17a,17b}$ = 13.0, $J_{17a,18}$ = 9.4)	41.7
17b	2.46, overlap	41.4	2.51, oveerlap	41.5	2.36, brd, ($J_{17a,17b}$ = 13.1)	41.7
18	3.96, m	43.0	3.97, m	43.1	3.97, m	42.6
18-NH	6.95, brd, ($J_{18,18\text{-NH}}$ = 7.9)		7.08, overlap		6.66, brd, ($J_{18,18\text{-NH}}$ = 7.7)	
19	0.98, d, ($J_{18,19}$ = 5.9)	20.7	0.97, d, ($J_{18,19}$ = 5.9)	20.9	1.04, d, ($J_{18,19}$ = 6.5)	20.1

Supplementary Table 3. Differences between the cyclic peptides and nemamide A in terms of ^{1}H and ^{13}C NMR chemical shifts.*

#	$\delta_{H(peptide)}$- $\delta_{H(nemamideA)}$			$\delta_{C(peptide)}$- $\delta_{C(nemamideA)}$		
	Cyclic Peptide **3** (2*S*,6*R*, 10*R*,18*R*)	Cyclic Peptide **4** (2*R*,6*S*, 10*R*,18*S*)	Cyclic Peptide **5** (2*R*,6*R*, 10*S*,18*S*)	Cyclic Peptide **3** (2*S*,6*R*, 10*R*,18*R*)	Cyclic Peptide **4** (2*R*,6*S*, 10*R*,18*S*)	Cyclic Peptide **5** (2*R*,6*R*, 10*S*,18*S*)
1				-1.4	-1.5	-1
2	-0.03	-0.02	-0.11	-0.2	-0.4	0.8
2-NH	0.03	0.39	0.03			
3a	-0.02	-0.02	0.11	-0.1	-1.8	-0.4
3b	0.01	0.08	-0.05	-0.1	-1.8	-0.4
4				-0.1	0.5	-0.1
4-NH_2a	-0.03	0	0.03			
4-NH_2b	-0.03	0.24	0.13			
5				-0.2	-0.4	0
6	-0.04	-0.05	-0.12	-0.1	-0.6	1.6
6-NH	-0.22	-0.61	0.47			
7a	0.02	-0.02	-0.08	-0.4	-0.5	-0.4
7b	0.03	0.1	-0.35	-0.4	-0.5	-0.4
8				0.3	0.5	-2.4
8-NH_2a	0.14	0.29	-0.29			
8-NH_2b	-0.06	0.06	-0.53			
9				0.2	-0.7	3.0
10	0.03	0.24	0.18	-0.4	-3.2	-1.6
10-NH	-0.23	-0.47	-0.38			
11a	0.07	0.04	-0.13	-0.3	-0.5	-0.3
11b	-0.02	0.12	-0.04	-0.3	-0.5	-0.3
12				0.5	-0.8	-2.8
12-NH_2a	0.01	0	0.03			
12-NH_2b	-0.15	-0.25	-0.18			
13				-0.1	-0.8	-1.1
14a	0.01	-0.05	-0.18	0.2	1.4	0.7
14b	0	-0.09	-0.01	0.2	1.4	0.7
15a	0.03	-0.01	0.18	0	-0.5	0.6
15b	0	0.13	-0.09	0	-0.5	0.6
15-NH	-0.37	-0.48	-0.73			
16				0.4	-0.1	-0.3
17a	-0.03	-0.07	-0.12	0.8	0.9	1.1
17b	-0.01	0.04	-0.11	0.8	0.9	1.1
18	-0.12	-0.11	-0.11	-1.9	-1.8	-2.3
18-NH	-0.1	0.03	-0.39			
19	-0.34	-0.35	-0.28	-23	-22.8	-23.6

* ^{1}H and ^{13}C NMR chemical shifts of nemamide A (listed in Supplementary Table 1) were subtracted from the corresponding chemical shifts of the three cyclic peptides (listed in Supplementary Table 2). If $\delta_{H(cyclic\ peptide)}$- $\delta_{H(nemamideA)} > 0.1$, the value is highlighted in red. If $\delta_{C(cyclic\ peptide)}$- $\delta_{C(nemamideA)} > 1$, the value is highlighted in red. Exchangeable protons are shaded light gray as their chemical shifts vary depending on sample concentration ([cyclic peptide] >> [nemamide A]) and other factors. C-1, C-18, and C-19 rows are shaded dark gray as these values should be quite different between nemamide A and the three cyclic peptides, as the cyclic peptides were all truncated versions of nemamide A.

Supplementary Table 4. Comparison of the A domain selectivity codes. Selectivity codes for β-Ala and L-Asn in bacterial A domains are listed (in red). The corresponding amino acids in the PKS-1 A_1, NRPS-1 A_2, and NRPS-1 A_3 domains are listed for comparison.

Sequence position:	235	236	239	278	299	301	322	330	331	517
β-Ala recognition	V	D	X	V	I	S	X	G	D	K
L-Asn recognition	D	L	T	K	L	G	E	V	G	K
PKS-1 A_1	D	V	S	F	T	G	I	I	W	K
NRPS-1 A_2	D	I	A	Y	Q	G	E	V	Y	K
NRPS-1 A_3	D	N	L	L	V	G	N	A	F	K

Supplementary Table 5. Primers used for plasmid construction or genotyping.

Primer	Purpose	Sequence (5'-3')*
nrps-1p-AscI-F	GFP reporter	gcatGGCGCGCCTGCATCAGCACATACTCAATGGTC
nrps-1p-NotI-R	GFP reporter	catgGCGGCCGCTGTGCAGAGTGCTCCGCGTAG
pks-1p-SalI-F	GFP reporter	gcgcGTCGACTGTGCATACATGAGTTGTTGCT
pks-1p-NotI-R	GFP reporter	catgGCGGCCGCTTTCTCCAAATCTTAATACAAATTATAT
nrps-1-F	Mos1 detection	GGAGAAGTCATCTGTTTCCA
nrps-1-R	Mos1 detection	TTGGCGATCACTTCAAATGG
pks-1-F	Mos1 detection	GAGGGAATATTGTATCCCACC
pks-1-R	Mos1 detection	GAAAACCGTGTTTGGTCTCG
oJL115[19]	Mos1 detection	GCTCAATTCGCGCCAAACTATG
daf-16-F[20]	deletion detection	GTAGACGGTGACCATCTAGAG
daf-16-internal[20]	deletion detection	CGGGAATTTCAGCCAAAGAC
daf-16-R[20]	deletion detection	GACGATCCAGGAATCGAGAG
unc-31-F	deletion detection	TAAGACCGCCCATGTTGCAC
unc-31-internal	deletion detection	AGTTGTGGCCTCTCCAATTC
unc-31-R	deletion detection	ATTCTGAGGGCACGACTCTG
ins-11-F	qRT-PCR	TCTTCGTCAATGAGGGTCAAG
ins-11-R	qRT-PCR	CAGTCGGATGCTGTTCTCC

*Underlined bases indicate restriction sites.

References

1 Weber, T. *et al.* antiSMASH 3.0-a comprehensive resource for the genome mining of biosynthetic gene clusters. *Nucleic Acids Res* (2015).

2 Gowda, H. *et al.* Interactive XCMS Online: simplifying advanced metabolomic data processing and subsequent statistical analyses. *Anal Chem* **86**, 6931-6939 (2014).

3 Nugroho, A. E. & Morita, H. Circular dichroism calculation for natural products. *J Nat Med* **68**, 1-10 (2014).

4 Lu, Z. *et al.* Cytotoxic polyphenols from the marine-derived fungus *Penicillium expansum*. *J Nat Prod* **73**, 911-914 (2010).

5 Wu, Q. X. *et al.* Azonazine, a novel dipeptide from a Hawaiian marine sediment-derived fungus, *Aspergillus insulicola*. *Org Lett* **12**, 4458-4461 (2010).

6 Liu, X. F. *et al.* Simplextones A and B, unusual polyketides from the marine sponge *Plakortis simplex*. *Org Lett* **13**, 3154-3157 (2011).

7 Kwan, D. H. & Schulz, F. The stereochemistry of complex polyketide biosynthesis by modular polyketide synthases. *Molecules* **16**, 6092-6115 (2011).

8 Reid, R. *et al.* A model of structure and catalysis for ketoreductase domains in modular polyketide synthases. *Biochemistry* **42**, 72-79 (2003).

9 Sievers, F. *et al.* Fast, scalable generation of high-quality protein multiple sequence alignments using Clustal Omega. *Mol Syst Biol* **7**, 539 (2011).

10 Kotowska, M. & Pawlik, K. Roles of type II thioesterases and their application for secondary metabolite yield improvement. *Appl Microbiol Biotechnol* **98**, 7735-7746 (2014).

11 Tamura, K., Stecher, G., Peterson, D., Filipski, A. & Kumar, S. MEGA6: Molecular Evolutionary Genetics Analysis version 6.0. *Mol Biol Evol* **30**, 2725-2729 (2013).

12 Baugh, L. R. & Sternberg, P. W. DAF-16/FOXO regulates transcription of *cki-1*/Cip/Kip and repression of *lin-4* during *C. elegans* L1 arrest. *Curr Biol* **16**, 780-785 (2006).

13 Fukuyama, M., Kontani, K., Katada, T. & Rougvie, A. E. The *C. elegans* Hypodermis Couples Progenitor Cell Quiescence to the Dietary State. *Curr Biol* **25**, 1241-1248 (2015).

14 Fukuyama, M., Rougvie, A. E. & Rothman, J. H. *C. elegans* DAF-18/PTEN mediates nutrient-dependent arrest of cell cycle and growth in the germline. *Curr Biol* **16**, 773-779 (2006).

15 Fukuyama, M. *et al. C. elegans* AMPKs promote survival and arrest germline development during nutrient stress. *Biol Open* **1**, 929-936 (2012).

16 Chen, Y. & Baugh, L. R. *Ins-4* and *daf-28* function redundantly to regulate *C. elegans* L1 arrest. *Dev Biol* **394**, 314-326 (2014).

17 Baugh, L. R. To grow or not to grow: nutritional control of development during *Caenorhabditis elegans* L1 arrest. *Genetics* **194**, 539-555 (2013).

18 Lee, B. H. & Ashrafi, K. A TRPV channel modulates *C. elegans* neurosecretion, larval starvation survival, and adult lifespan. *PLoS Genet* **4**, e1000213 (2008).

19 Boulin, T. & Bessereau, J. L. Mos1-mediated insertional mutagenesis in *Caenorhabditis elegans*. *Nat Protoc* **2**, 1276-1287 (2007).

20 Jeong, M. H., Kawasaki, I. & Shim, Y. H. A circulatory transcriptional regulation among *daf-9*, *daf-12*, and *daf-16* mediates larval development upon cholesterol starvation in *Caenorhabditis elegans*. *Dev Dyn* **239**, 1931-1940 (2010).